ESC European Society of Cardiology

Cardiovascular Research (2023) **119**, 1981–1996
https://doi.org/10.1093/cvr/cvad105

Lipocalin 10 is essential for protection against inflammation-triggered vascular leakage by activating LDL receptor-related protein 2-slingshot homologue 1 signalling pathway

Hongyan Zhao[1,2], Peng Wang[2,3], Xiaohong Wang[2], Wa Du[4], Hui-Hui Yang[2], Yueying Liu[2], Shu-Nan Cui[2,5], Wei Huang[6], Tianqing Peng[7], Jing Chen[8], Chen Gao[2], Yigang Wang[6], Sakthivel Sadayappan[9], Chengen Ma[1], Yanbo Fan[4], Chunting Wang[3], and Guo-Chang Fan[2]*

[1]Department of Critical Care Medicine, The Second Hospital, Cheeloo College of Medicine, Shandong University, Jinan, Shandong, China; [2]Department of Pharmacology and Systems Physiology, University of Cincinnati College of Medicine, 231 Albert Sabin Way, Cincinnati, OH 45267-0575, USA; [3]Department of Critical Care Medicine, Shandong Provincial Hospital Affiliated to Shandong First Medical University, Jinan, Shandong, China; [4]Department of Cancer Biology, University of Cincinnati College of Medicine, Cincinnati, OH, USA; [5]Department of Anesthesiology, Beijing Cancer Hospital, Peking University School of Oncology, Beijing, China; [6]Department of Pathology and Laboratory Medicine, University of Cincinnati College of Medicine, Cincinnati, OH, USA; [7]The Centre for Critical Illness Research, Lawson Health Research Institute, London, Ontario, Canada; [8]Division of Biomedical Informatics, Cincinnati Children's Hospital Medical Center, Cincinnati, OH, USA; and [9]Division of Cardiovascular Health and Disease, Department of Internal Medicine, University of Cincinnati College of Medicine, Cincinnati, OH, USA

Received 16 September 2022; revised 6 March 2023; accepted 20 March 2023; online publish-ahead-of-print 1 July 2023

Time of primary review: 49 days

Aims

Systemic inflammation occurs commonly during many human disease settings and increases vascular permeability, leading to organ failure, and lethal outcomes. Lipocalin 10 (Lcn10), a poorly characterized member of the lipocalin family, is remarkably altered in the cardiovascular system of human patients with inflammatory conditions. Nonetheless, whether Lcn10 regulates inflammation-induced endothelial permeability remains unknown.

Methods and results

Systemic inflammation models were induced using mice by injection of endotoxin lipopolysaccharide (LPS) or caecal ligation and puncture (CLP) surgery. We observed that the expression of Lcn10 was dynamically altered only in endothelial cells (ECs), but not in either fibroblasts or cardiomyocytes isolated from mouse hearts following the LPS challenge or CLP surgery. Using *in vitro* gain- and loss-of-function approaches and an *in vivo* global knockout mouse model, we discovered that Lcn10 negatively regulated endothelial permeability upon inflammatory stimuli. Loss of Lcn10 augmented vascular leakage, leading to severe organ damage and higher mortality following LPS challenge, compared to wild-type controls. By contrast, overexpression of Lcn10 in ECs displayed opposite effects. A mechanistic analysis revealed that both endogenous and exogenous elevation of Lcn10 in ECs could activate slingshot homologue 1 (Ssh1)-Cofilin signalling cascade, a key axis known to control actin filament dynamics. Accordingly, a reduced formation of stress fibre and increased generation of cortical actin band were exhibited in Lcn10-ECs, when compared to controls upon endotoxin insults. Furthermore, we identified that Lcn10 interacted with LDL receptor-related protein 2 (LRP2) in ECs, which acted as an upstream factor of the Ssh1-Confilin signalling. Finally, injection of recombinant Lcn10 protein into endotoxic mice showed therapeutic effects against inflammation-induced vascular leakage.

Conclusion

This study identifies Lcn10 as a novel regulator of EC function and illustrates a new link in the Lcn10-LRP2-Ssh1 axis to controlling endothelial barrier integrity. Our findings may provide novel strategies for the treatment of inflammation-related diseases.

* Corresponding author. Tel: +(513)558 2340; fax: +(513)558 9969, E-mail: fangg@ucmail.uc.edu

Graphical Abstract

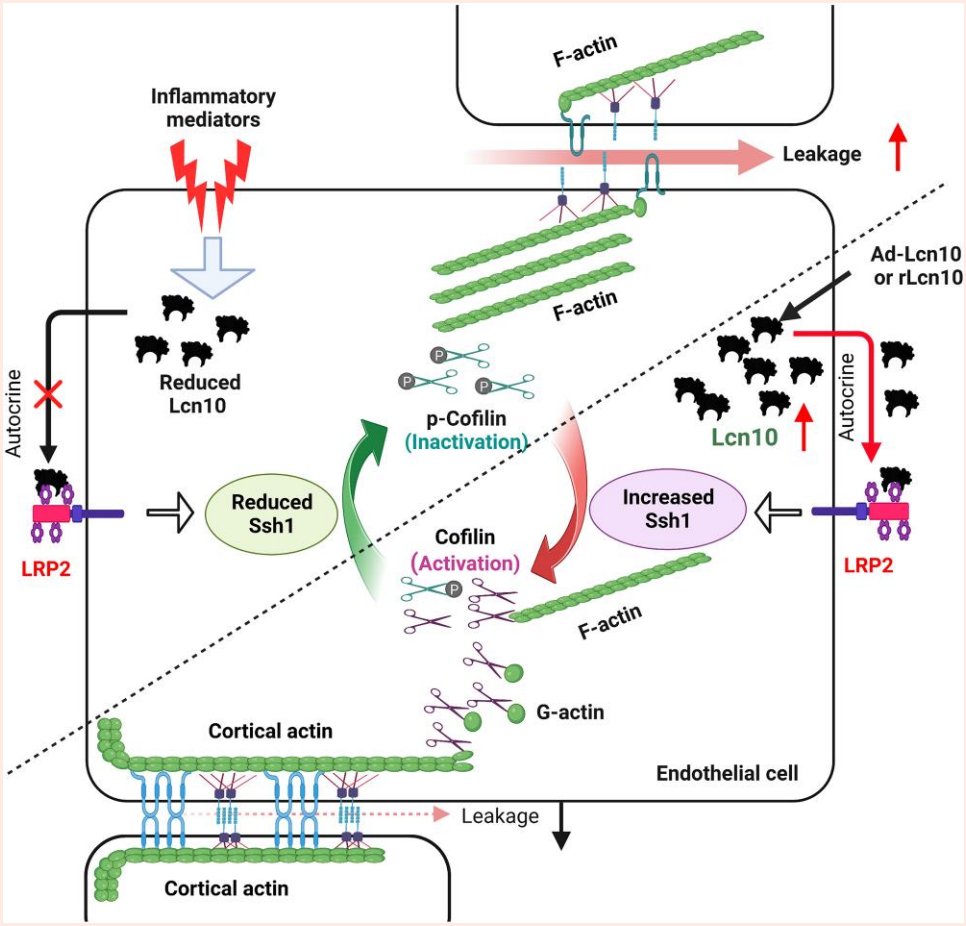

Keywords Lcn10 • Endothelial permeability • Systemic inflammation • Actin filament • Ssh1

1. Introduction

Systemic inflammation occurs commonly with many human disease conditions ranging from COVID-19, bacterial sepsis to sterile syndromes such as cardiopulmonary bypass surgery, reperfusion injury, and protein/antibody drug toxicity.[1–3] As a result, blood vessels are constantly sensing and responding to these systemic inflammatory stimuli, which promotes a loss of endothelial barrier integrity and increases the permeability of endothelial monolayer, leading to tissue oedema, hypotension, organ failure, and eventually lethal outcomes.[4–6] For example, septic patients often develop a progressive accumulation of oedema fluid in the interstitial spaces, subcutaneous tissue, and body cavities, which suggests the disruption of endothelial integrity and increased vascular leakage during sepsis.[7] Indeed, systemic inflammation-triggered vascular hyper-permeability has been well considered as a key contributor to the increased mortality in the critical care unit. Unfortunately, therapies targeting the increased vascular permeability during systemic inflammation have been ineffective thus far.[8] Hence, it will be of great significance to better understand the pathogenesis of vascular leakage and explore the most effective therapies for the treatment of vascular hyper-permeability.

The current paradigm states that the increase of vascular leakage is driven, on the one hand, by the generation of the centripetal contractile forces in endothelial cells (ECs) and, on the other hand, by the loss of EC junctional integrity, provided mostly by the tight and adherence junctions.[9–11] Both endothelial contraction and the maintenance of junctional integrity depend on actin filament re-organization.[9] Notably, there are two forms of actin known to exist in ECs including monomeric globular actin (G-actin) and polymerized filamentous actin (F-actin).[9] Under resting conditions, a subset of G-actin monomers assemble along the cell periphery as cortical actin filaments, which connect to transmembrane junction proteins [i.e. Occludin and vascular endothelial (VE)-cadherin]) for maintaining barrier integrity.[10] During systemic inflammation (i.e. sepsis), inflammatory mediators disturb normal actin dynamics, leading to increased actin fibre bundling and stress-fibre formation that generate pulling forces and compromise EC contact stability.[10] Hence, the modification of actin filament dynamics in ECs could be a valuable approach to the development of treatment options for vascular leakage. Research over the past decade has focused on two major pathways, including those associated with small GTPases and those associated with myosin light chain (MLC) kinases/phosphatases that control actin dynamics and cell contraction.[12–14] However, another key signalling pathway involving LIM kinases (LIMKs) and their downstream target, Cofilin, has been less well studied in sepsis-induced vascular leakage. At present, there is evidence that Cofilin depolymerizes F-actin to provide new G-actin monomers for polymerization.[15] In addition, Cofilin activity is tightly controlled by LIM-domain containing kinase (LIMK)1/2, which phosphorylates Cofilin and blocks its activity.[16] By contrast, dephosphorylation by the slingshot homologue 1 (Ssh1) phosphatase

can reactivate Cofilin, which stimulates the severance and depolymerization of F-actin filaments.[9,17] Therefore, any mediators that either reduce LIMK1/2 or increase Ssh1 levels would be beneficial for protection against vascular leakage.

The lipocalin (LCN) family proteins share a common three-dimensional structure consisting of an eight-stranded antiparallel β-barrel.[18] They are secreted proteins that can be detected in plasma and other body fluids.[18] Accordingly, several human lipocalins have been used clinically as biochemical markers for the diagnosis of various diseases.[19–21] For example, Lipocalin 2 (Lcn2), also referred to as neutrophil gelatinase-associated LCN (NGAL), is clinically utilized as a biomarker for acute and chronic renal injury.[21] Recently, Apolipoprotein M (ApoM) and Lcn2 (two members of LCN family) have garnered attention in the regulation of vascular inflammation and permeability.[22–25] For instance, multiple groups have observed that ApoM, as a main carrier of plasma sphingosine 1-phosphate (S1P), is critical for the maintenance of vascular integrity and inhibition of vascular inflammation through the activation of S1P receptor 1-signalling in ECs.[23–25] However, whether other lipocalins play a role in the regulation of endothelial permeability remains unknown. More intriguingly, two lipocalins, Lcn2 and Lcn10, exhibit an opposite expression pattern upon sterile and non-sterile inflammatory conditions.[26–30] Through RNA-sequencing (RNA-seq) of peripheral blood RNA samples collected from 129 sepsis patients, Tsalik *et al.* reported that Lcn2 was significantly higher in sepsis non-survivors than sepsis survivors.[28] Conversely, Lcn10 was increased dramatically in sepsis survivors than in non-survivor counterparts.[28] In the cardiac disease settings, both systemic and myocardial expression of Lcn2 are increased in clinical and experimental failing hearts.[29] By contrast, using a quantitative meta-analysis of three cardiac RNA-seq datasets, Alimadadi *et al.* reported that Lcn10 is one of the three common differentially expressed genes and is the most significantly downregulated gene (reduced by 2.14-fold) in heart tissues from patients with dilated cardiomyopathy.[30] We also found that the expression pattern of Lcn2 and Lcn10 is inversely regulated in macrophages upon inflammatory stimuli.[31] Unlike Lcn2, a well-characterized member of LCN family for its role in inflammatory diseases[32] and metabolic disorders,[33] the current understanding of Lcn10 function is very limited. Hence, these divergent phenomena of Lcn2 and Lcn10 listed above sparked our curiosity to explore whether Lcn10 plays a role in inflammation-induced vascular leakage.

In this study, we provide the first evidence showing that Lcn10 is a potent and novel regulator of vascular permeability and has potential as an innovative protector against inflammation-triggered vascular leakage and heart failure.

2. Methods

2.1 Animal models

C57BL/6 (Wild-type, WT) mice were purchased from Jackson Laboratory (Bar Harbor, ME). Lcn10-knockout (KO) (C57BL/6N-LCN10tm1.1) mice were obtained from the University of California, Davis (Davis, CA). All these mice were bred in the Division of Laboratory Animal Resources at the University of Cincinnati Medical Center. Endotoxin-induced systemic inflammatory mouse model was established in both WT and Lcn10-KO mice by intraperitoneal injection of lipopolysaccharide (LPS) (10 mg/kg BW). Polymicrobial sepsis was surgically induced by caecal ligation and puncture (CLP) as previously described.[34] Mice were anaesthetised by intraperitoneal injection with a mixture of ketamine (100 mg/kg) and xylazine (5 mg/kg), and depth of anaesthesia was monitored by toe pinch. All animal experiments conformed to the Guidelines for the Care and Use of Laboratory Animals prepared by the National Academy of Sciences, published by the National Institutes of Health, and approved by the University of Cincinnati Animal Care and Use Committee (Protocol #21-08-06-01).

2.2 Isolation and culture of mouse cardiac ECs, myocytes, and fibroblasts

Primary cardiac ECs were isolated from mice as described previously.[35] Primary cardiomyocytes and fibroblasts were isolated from WT, LPS- or CLP-treated septic mice following the protocol described previously.[36] A mouse cardiac endothelial cell line (MCEC) was purchased from CELLutions Biosystems Inc. (Burlington, ON, Canada).

2.3 Infection/transfection MCECs with adenoviral vectors or siRNAs

MCECs were seeded and allowed to reach 50–70% confluency by the time of infection with adenoviral (Ad) vectors (Ad.GFP-Lcn10, or Ad.GFP) for 1 h, followed by incubation for 36–48 h. These Ad-infected cells were harvested for RT-qPCR, RNA-seq, and Western blot analysis, or subjected to inflammatory stimuli to determine the permeability. For the small interfering RNA (siRNA) transfection experiment, MCECs (1×10^5 cells/well) were seeded on a six-well plate and allowed to reach 40–50% confluency. Then MCECs were transfected with 50 nM siRNA oligonucleotides for 48–60 h, using the lipofectamine 3000 reagents according to the manufacturer's instructions.

2.4 RT-qPCR, RNA-Seq, bioinformatic assay, and gene set enrichment analysis

All primer sets are listed in the Supplementary material online, *Table S1*. Gene expression was normalized to the housekeeping gene 18S and relative fold expression for target genes was calculated by the $2^{-\Delta\Delta Ct}$ method. RNA-sequencing analysis was performed by the Genomics, Epigenomics, and Sequencing Core (GESC) at the University of Cincinnati. The library was aligned and quantified using STAR V.2.6.1. FASTQ files were generated using bcl2fastq (Illumina). Reads were aligned to the mm10 genome assembly using R subread (V.2.8.2). Counts were then summarized at the gene level using feature counts and normalized using Deseq2 (V.1.34.0). Differentially expressed genes (absolute log2-fold change of greater than 0; false-discovery rate (FDR)-adjusted *P*-value of less than 0.1) were identified with the DESeq2. Gene set enrichment analysis (GSEA) was performed using GSEA software (v. 4.2.3) to compare gene expression signatures between Ad.Lcn10– and control Ad.GFP-MCECs. Actin cytoskeleton organization and cell-cell Junction-related gene sets were selected from the Molecular Signatures Database (MSigDB version 7.5.1). GSEA scores were calculated for sets with a minimum of ten detected genes, all other parameters were default.

2.5 *In vitro* endothelial permeability assays

MCEC permeability was monitored at different time points after treatment with LPS (10 ug/mL), TNFα (10 ng/mL) or PBS vehicle by measuring: (i) values of trans-endothelial electrical resistance (TEER) using an EVOM2 volt-ohmmeter (World Precision Instruments, Sarasota, FL) according to our previous descriptions;[37] (ii) Fluorescein isothiocyanate (FITC)-dextran and Evans blue dye (EB)-albumin flux assays,[38] as detailed in Supplementary material online, Methods.

2.6 *In vivo* vascular permeability, tissue oedema, and organ damage assays

For *in vivo* vascular permeability analysis, Lcn10-KO and WT mice (8-week-old, male) were injected intraperitoneally (IP) with LPS (10 μg/g BW). For testing the therapeutic effects of recombinant Lcn10 protein (rLcn10) in LPS-induced vascular leakage, WT mice (5–6-week-old) were injected i.p. with LPS (10 μg/g BW). One hour later, rLcn10 (0.2 μg/g BW) or PBS (control) was injected via the tail vein. At 20 h post-LPS injection, 0.5% EB dye in PBS (40 μg/g BW) was injected via the tail vein. One hour later, the mice were perfused with PBS containing 2 mM ethylenediaminetetraacetic acid (EDTA) to flush out the blood and EB in the vessels after anaesthesia. Then organs including the heart, aorta, lung, stomach, intestine, liver, spleen, and kidney were harvested and weighed, and for the subsequent permeability analysis, as detailed in Supplementary material online, Methods.

2.7 Measurement of cardiac function

Cardiac function was assessed by performing transthoracic M-model echocardiography with a 30 MHz linear array transducer as previously described.[39]

2.8 Western-blotting, immunofluorescence staining, and protein–protein binding ELISA

Mouse hearts were harvested at the indicated time points after LPS injection or CLP and lysed in NP-40 lysis buffer containing 0.1 mM phenylmethylsulfonyl fluoride (PMSF), a protease inhibitor cocktail. MCECs infected with adenovirus vectors or transfected with siRNAs were collected and lysed in radio-immunoprecipitation assay containing 0.1 mM PMSF, protease inhibitor cocktail, and 1% phosphatase inhibitor cocktail. Equal amounts of protein samples (60–120 μg) were loaded to 10–12% SDS-PAGE for western-blotting analysis, as detailed in Supplementary material online, *Methods*. The Immunostaining assays of actin filament dynamics in MCECs and co-localization of LRP2 and Lcn10 in MCECs are detailed in Supplementary material online, *Methods*. Protein–protein binding ELISA assay was performed to test the interaction of LRP2 with Lcn10 *in vitro*, as we described previously[40] and detailed in Supplementary material online, *Methods*.

2.9 Statistical analysis

GraphPad Prism 8 (GraphPad Software, San Diego, CA, USA) was utilized for statistical analysis. Data were presented as means ± SEM. Significance was determined by Student's *t*-test and 1- or 2-way analysis of variance (ANOVA) to determine differences within groups where appropriate. Survival was presented as Kaplan–Meier curves and differences were analysed by the log-rank test in GraphPad Prism software. $P < 0.05$ was considered statistically significant.

3. Results

3.1 The expression of Lcn10 is markedly altered in ECs under septic challenge

Lcn10 was initially identified as an epididymal gene.[41] However, recent genome-wide RNA sequencing analysis of human tissues showed that Lcn10 is also expressed in other tissues such as the heart, spleen, and thyroid. Similarly, using the Western-blotting approach to determine its tissue distribution in mice, we observed that protein levels of Lcn10 were enriched in whole blood cells, spleen, and heart (see Supplementary material online, *Figure S1*). Interestingly, recent clinical data on the alteration of Lcn10 levels in patients with cardiac inflammation appears controversial, which reveals the increased serum Lcn10 levels in patients with sepsis-induced cardiomyopathy,[27] but reduced expression in human failing hearts.[30] To clarify this concern, we first measured cardiac expression levels of Lcn10 in mice at different time points after endotoxin LPS injection or CLP surgery. As shown in *Figure 1A* and *B*, protein levels of Lcn10 were significantly increased in mouse hearts at 3 and 6 h post-LPS injection, whereas were remarkably decreased at 24 h post-LPS treatment, compared to control samples. Consistently, cardiac Lcn10 levels were mildly elevated in mice at 12 h post-CLP surgery but were greatly declined in mice at 48 h post-CLP, compared to sham-operated controls (*Figure 1C* and *D*). In parallel, we determined mRNA levels of Lcn10 in these LPS- and CLP-treated mouse hearts, using RT-qPCR. Our results showed that Lcn10 mRNA levels were greatly increased at 3 h, peaked at 6 h, and then significantly reduced at 24 h post-LPS injection (*Figure 1E*). CLP surgery caused a significant upregulation of cardiac Lcn10 mRNA at 12 h, but not at 24 h, and that was markedly decreased at 48 h post-CLP, compared to sham-operated samples (*Figure 1F*).

Given that the top three cell populations within mouse myocardium are ECs (29%), fibroblasts (25%), and cardiomyocytes (23%),[42] we therefore determined whether such inflammation-induced alterations of Lcn10 expression occurred equally or differently in these three cardiac cell populations. Surprisingly, we observed that LPS-caused elevation and reduction of cardiac Lcn10 mRNA levels occurred only in ECs but not in fibroblasts or cardiomyocytes (*Figure 1G*). Similar results were also demonstrated in three cardiac cell types isolated from mice at different time points post-CLP surgery (*Figure 1H*). Furthermore, we cultured mouse cardiac endothelial cells (MCECs), cardiac myocytes (MCMs), and fibroblasts (MCFs) *in vitro* to determine the dynamic expression of Lcn10 in response to inflammatory stimuli. We observed that the expression of Lcn10 was significantly upregulated at 6 h and then reduced or returned to normal levels at 24 h in both LPS- and TNFα-treated MCECs but not in either MCFs or MCMs upon the addition of LPS or TNFα (*Figure 1I* and *J*). Together, both *in vivo* and *in vitro* results consistently indicate that the expression of Lcn10 is dynamically altered in ECs during sepsis. It suggests that Lcn10 may be strongly correlated with inflammation-triggered vascular permeability.

3.2 Knockdown of Lcn10 in ECs aggravates the inflammation-induced permeability

Considering the expression of endothelial Lcn10 is elevated at the early phase but is reduced at the late phase of systemic inflammation (*Figure 1*), we then hypothesized that Lcn10 is required for ECs to maintain endothelial barrier integrity upon inflammation insults. To test this hypothesis, we transfected ECs with two siRNAs specific to Lcn10 (si-Lcn10–1 and si-Lcn10-2), separately. RT-qPCR analysis results showed that mRNA levels of Lcn10 were significantly reduced in both si-Lcn10-1- and si-Lcn10-2-transfected ECs, compared to control siRNA (si-Ctl)-transfected cells upon basal PBS-treated conditions (*Figure 2A* and *B*). Importantly, both LPS- and TNFα-induced transient upregulation of Lcn10 was also remarkably blocked by these Lcn10-siRNAs, as evidenced by higher levels of Lcn10-mRNA in control siRNA-ECs, but not in either Lcn10-siRNA-transfected cells after treatment with LPS- and TNFα for 6 h (*Figure 2A* and *B*).

Next, we determined whether the reduction of Lcn10 altered EC integrity upon inflammation conditions. 24-h after transfected with siRNAs, ECs were collected and re-seeded onto 12-mm Transwell with 0.4 μm-pore polyester membrane insert. When a cell monolayer was formed, LPS (10 μg/mL) or TNFα (10 ng/mL) was added to the chamber and then permeability was measured using the following three methods: (i) TEER values; (ii) FITC-dextran flux; and (iii) EB dye-albumin flux assays. It is important to note here that there was no difference in basal barrier function between control si-Ctl-transfected ECs and si-Lcn10-1/2-transfected cells (see Supplementary material online, *Figure S2A–C*). However, LPS-caused drops of TEER values, observed in si-Ctl-transfected cells, were significantly aggravated in both si-Lcn10-groups (*Figure 2C*). These data indicate that the reduction of Lcn10 promotes LPS-induced endothelial permeability. Furthermore, the fluxes of FITC-dextran from the upper chamber to the lower chamber were significantly increased in both si-Lcn10-groups, compared to siRNA-controls during 2–3 h after the LPS challenge (*Figure 2D*). Consistently, the leakage of EB-albumin from the upper to the lower chamber was more pronounced in si-Lcn10-groups than siRNA-controls at 2 and 3 h post-LPS stimulation (*Figure 2E*). Similar results were also observed in ECs challenged with TNFα, as indicated by significantly lower values of TEER (*Figure 2F*) and significantly higher fluxes of FITC-dextran and EB- albumin in si-Lcn10-transfected ECs than siRNA-controls after TNFα insults (*Figure 2G* and *H*). Put together, these *in vitro* data suggest that Lcn10 is essential for ECs to maintain barrier integrity and accordingly, loss of Lcn10 would promote inflammation-triggered endothelial leakage.

3.3 Lcn10-deficiency exaggerates vascular leakage, organ injury, and animal mortality upon systemic inflammation challenge

To test the *in vivo* effects of Lcn10-deficiency in vascular permeability and organ injury during systemic inflammation, we utilized a global Lcn10-KO mouse model and induced systemic inflammation by intraperitoneal injection of LPS (10 mg/kg BW). Generation of Lcn10-KO mice was confirmed by PCR genotyping (*Figure 3A*) and Western blotting (*Figure 3B*). It is

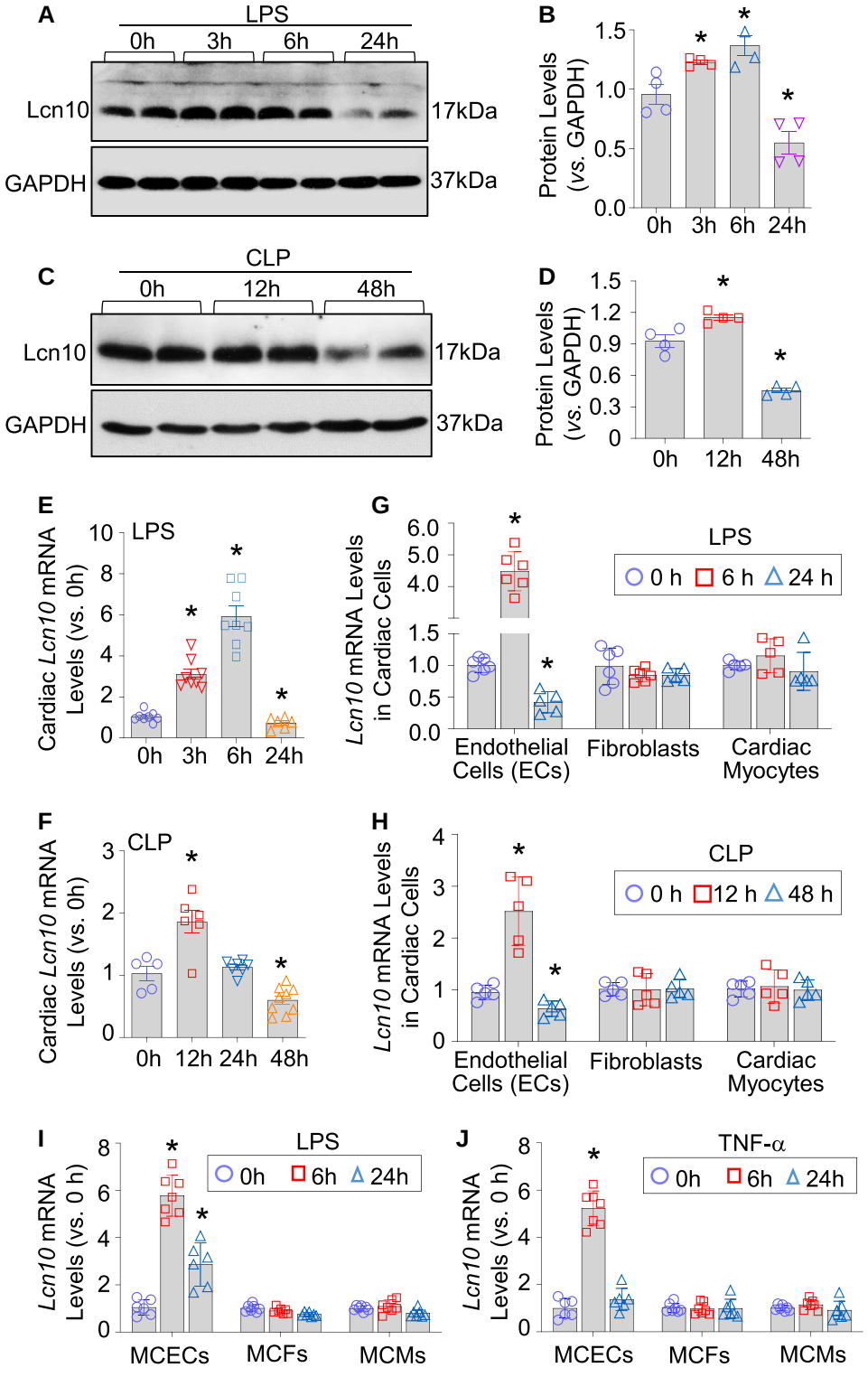

Figure 1 The dynamic expression of Lcn10 in cardiovascular cells upon inflammatory challenge. (*A* and *B*) Representative immunoblots and their quantification analysis for measuring cardiac Lcn10 levels in mice after intraperitoneal injection of LPS (10 mg/kg BW) ($n = 4$). (*C* and *D*) Representative immunoblots and their quantification analysis for measuring cardiac Lcn10 levels at the indicated time points after CLP surgery ($n = 4$). (*E*) RT-qPCR analysis of Lcn10 mRNA levels in mouse hearts collected at 0, 3, 6, and 24 h post-LPS injection (10 mg/kg BW) ($n = 6$–8). (*F*) Lcn10 mRNA levels were determined by RT-qPCR in mouse hearts collected at 0, 12, and 48 h after CLP ($n = 5$–9). (*G* and *H*) ECs, cardiomyocytes, and fibroblasts were, respectively, isolated from mouse hearts at the indicated time points post-LPS injection (*G*) and post-CLP surgery (*H*), then total RNAs were collected and assessed Lcn10 expression by RT-qPCR ($n = 5$–6). (*I* and *J*) mRNA levels of Lcn10 were measured in cultured MCECs (mouse cardiac endothelial cells), MCFs, and MCMs at the indicated time points after stimulation with LPS (10 μg/mL) (*I*) and TNFα (10 ng/mL) (*J*) ($n = 6$–7; *$P < 0.05$). Glyceraldehyde-3-phosphate dehydrogenase (GAPDH) was used as an internal loading control for Western-blotting, and 18s-RNA expression was used as the internal control for RT-qPCR. All results are presented as mean ± SEM and analysed by student's *t*-test (*$P < 0.05$).

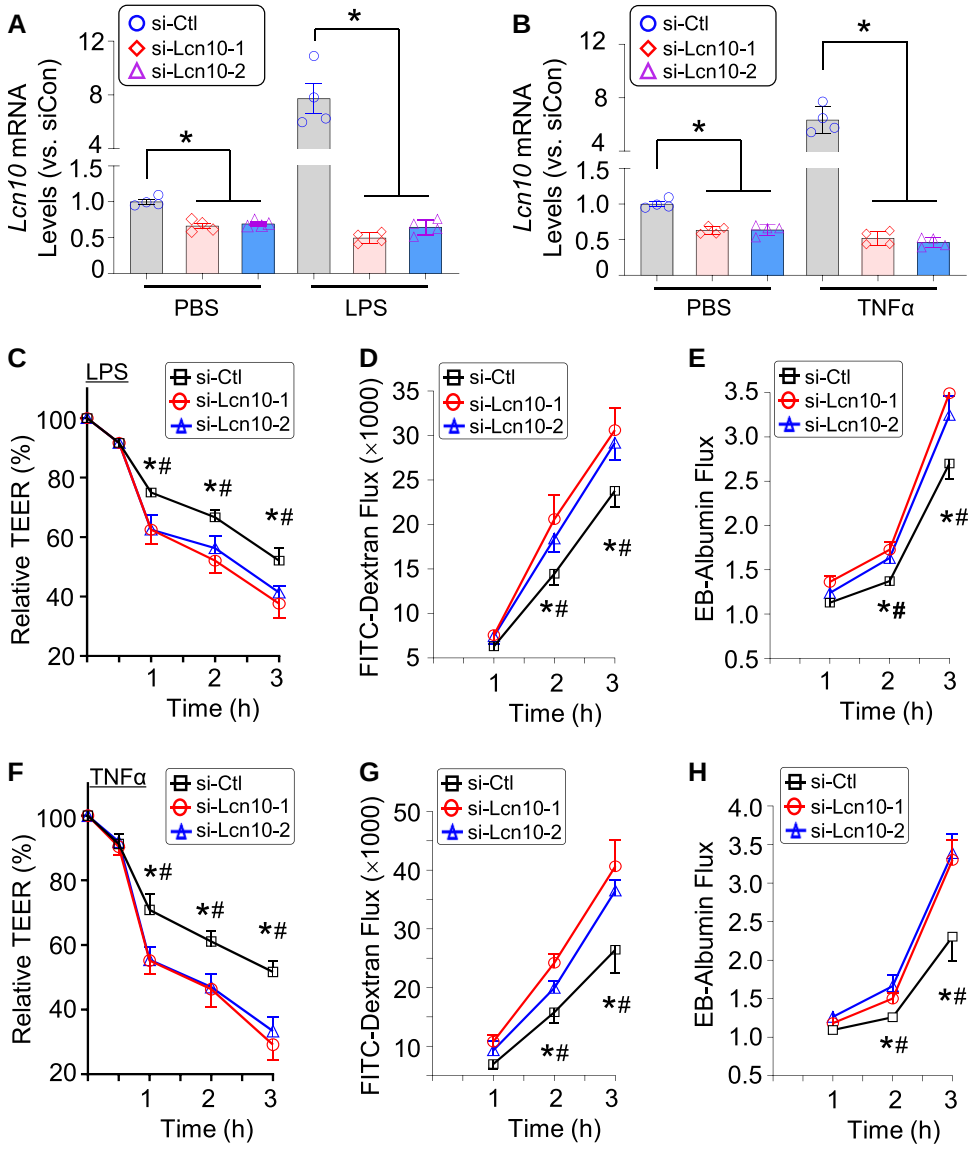

Figure 2 Lcn10 deficiency augments the inflammation-induced EC monolayer leakage. (*A* and *B*) Mouse cardiac ECs (MCECs) were transfected with si-Lcn10-1, si-Lcn10-2, and control siRNA (si-Ctl). Sixty hours later, these transfected cells were treated with PBS, LPS (10 μg/mL), or TNFα (10 ng/mL) for 3 h and then isolated total RNA for RT-qPCR analysis of Lcn10 expression ($n = 4$). Results are presented as mean ± SEM and analysed by student's *t*-test (*$P < 0.05$). (*C–E*) EC-monolayer permeability was measured in si-Lcn10-transfected cells and controls after LPS stimulation by (*C*) TEER, (*D*) FITC-dextran, and (*E*) EB-BSA flux ($n = 4–6$; *$P < 0.05$, si-Lcn10-1 vs. si-Ctl; #$P < 0.05$, si-Lcn10-2 vs. si-Ctl). (*F–H*) EC-monolayer permeability was measured in si-Lcn10-transfected cells and controls after treatment with TNFα by (*F*) TEER, (*G*) FITC-dextran, and (*H*) EB-BSA flux ($n = 4–6$; *$P < 0.05$, si-Lcn10-1 vs. si-Ctl; #$P < 0.05$, si-Lcn10-2 vs. si-Ctl). Similar results were obtained in the other two independent experiments. Results in (*C–H*) are presented as mean ± SD and analysed by two-way analysis of variance (ANOVA) (*$P < 0.05$).

important to note here that Lcn10-KO mice are healthy and do not display any obvious cardiac pathological abnormalities, as evidenced by no differences in the ratio of heart weight (HW)/body weight (BW), cardiac chamber structure, cardiomyocyte cross-sectional area, and cardiac capillary density between WT and Lcn10-KO mice (see Supplementary material online, *Figure S3A–E*). However, these Lcn10-KO mice showed severer vascular leakage in response to LPS-triggered systemic inflammation, as evidenced by the following experimental results. First, when 0.5% EB dye was intravenously administered to mice (4 mg/kg BW) at 20 h post-LPS injection, Lcn10-KO mice displayed poorer peripheral circulation (less blue dye on lips and extremities) than WT mice (*Figure 3C*). Clinically, the peripheral circulation in septic patients is closed to ensure the blood supply of important organs, and less peripheral perfusion is correlated to the severity of sepsis.[43] Indeed, further analysis of EB dye leakage within organs, we observed that Lcn10-KO mice showed organ oedema, as evidenced by enlarged organ size and increased extravasation of the dye in the heart (*Figure 3D*) and aorta (*Figure 3E*) as well as the lung (see Supplementary material online, *Figure S3F*), intestine (see Supplementary material online, *Figure S3G*), and stomach (see Supplementary material online, *Figure S3H*), compared to WT samples. For quantitative analysis, we incubated these organs in formamide at 55°C for 48 h to elute EB dye, followed by measuring the optical density at 620 nm on a spectrophotometer. Our results showed that the extravasation of EB dye was significantly elevated by 2.0-fold in hearts (*Figure 3F*), 1.7-fold in aortas (*Figure 3G*), 2.2-fold in

lungs (see Supplementary material online, *Figure S3I*), 1.4-fold in the intestine (see Supplementary material online, *Figure S3J*), and 1.8-fold in the stomach (see Supplementary material online, *Figure S3K*), collected from LPS-treated KO mice, compared to WT controls. We also measured the EB dye extravasation in the liver, spleen, and kidney, which showed no significant difference between KO and WT groups (see Supplementary material online, *Figure S3L*). Next, we analysed frozen organ sections under a confocal fluorescence microscope and the extravasated EB dye within the tissue interstitial space became red. Using Image J software, we quantified the relative intensity of red fluorescence and showed that the interstitial extravasation of EB dye was significantly elevated by 1.4-fold in hearts (*Figure 3H* and *I*) and 1.5-fold in aortas (*Figure 3J* and *K*) collected from Lcn10-KO mice, compared to WT group (*Figure 3J* and *K*). Similarly, the EB dye extravasation in the intestine and the stomach of LPS-treated KO mice was also significantly increased, compared with WT samples (see Supplementary material online, *Figure S3M and N, O and P*). Finally, we quantified the degree of tissue oedema in these organs of Lcn10-KO and WT mice upon LPS challenge. As shown in Supplementary material online, *Figure S3Q*, LPS-treated KO-mice exhibited a higher ratio of wet weight/dry weight in the lung and intestine, while not in the liver, spleen, and kidney. Taken together, the above multiple lines of evidence strongly indicate that Lcn10 deficiency causes vascular hyper-permeability upon systemic inflammatory conditions.

Next, we examined whether increased vascular leakage in LPS-KO mice could aggravate organ injury. As expected, the lung tissues collected from LPS-KO mice significantly increased: (i) the thickness of the alveolar wall, (ii) formation of hyaline membranes, and (iii) the alveolar collapse, compared to LPS-WT samples (see Supplementary material online, *Figure S3R*). Accordingly, the total injury score in the lung of LPS-KO mice was greatly higher than LPS-WT controls (see Supplementary material online, *Figure S3S*). In addition, histological analyses also showed that Lcn10 deficiency significantly augmented LPS-induced gut injury, as evidenced by a significant decrease in the villus length (see Supplementary material online, *Figure S3T*) and an apparent increase in the Chiu's score (see Supplementary material online, *Figure S3U*), compared to LPS-WT controls. Furthermore, using echocardiography, we determined cardiac function in LPS-treated KO and WT mice. As shown in *Figure 3L–Q* and Supplementary material online, *Table S2*, injection of LPS to WT mice resulted in poorer myocardial contractile function, which is consistent with previous findings;[39,44] however, such LPS-induced cardiac dysfunction was more pronounced in Lcn10-KO mice, which was evidenced by a significant lower of ejection fraction (EF%) (*Figure 3P*) and fractional shortening (FS%) (*Figure 3Q*), compared to WT-controls. Given that multi-organ injury, especially cardiac depression represents the major cause of death in systemic inflammation,[39,44] we, therefore, monitored animal survival after the LPS challenge. As shown in *Figure 3R*, Lcn10-KO mice exhibited a lower survival rate (10%) than WT mice (40%) at 96 h post-LPS injection. Collectively, these results indicate that Lcn10 depletion in mice appears more sensitive to systemic inflammation-induced vascular permeability, leading to severe multiple organ damage and eventually, animal death.

3.4 Overexpression of Lcn10 in ECs counteracts inflammation-triggered hyper-permeability

To further determine the role of Lcn10 in the regulation of endothelial barrier integrity, we next utilized a gain-of-function approach to overexpress Lcn10 in ECs through transfection with Ad.Lcn10. Ad.GFP-infected ECs were used as control. Please note here that Ad.Lcn10 vector contains two independent expression cassettes one is for mouse Lcn10 gene expression, and another is for GFP expression. Gene transfer efficiency was assessed by GFP fluorescence at 24 h post-infection (*Figure 4A*). In addition, RT-qPCR results showed that mRNA levels of Lcn10 were dramatically increased in Ad.Lcn10-infected ECs, compared to Ad.GFP-cells (*Figure 4B*). Subsequently, these Ad-infected ECs were harvested and re-seeded onto 12-mm Transwell with 0.4 μm-pore, followed by treatment with LPS (10 μg/mL) or TNFα (10 ng/mL) for measuring endothelial permeability. We observed that LPS-induced drops of TEER values in Ad.GFP-ECs were remarkably attenuated in Ad.Lcn10-ECs (*Figure 4C*), suggesting more resistance to LPS-caused leakage in Lcn10-overexpressing cells. Furthermore, both FITC-dextran and EB-albumin flux assays consistently revealed that Ad.Lcn10-ECs displayed lower leakage of these fluorescence dyes through the endothelial monolayer, compared to Ad.GFP-controls (*Figure 4D* and *E*). Similarly, TNFα-induced disruption of EC barrier integrity was greatly suppressed in Ad.Lcn10-cells, as evidenced by less reduction of TEER (*Figure 4F*) as well as less fluxes of FITC-dextran (*Figure 4G*) and EB-albumin dyes (*Figure 4H*), in comparison with Ad.GFP-cells.

Finally, it would be argued whether the Lcn10-mediated reduction of EC permeability was due to its impact on cell viability or cell damage. Therefore, we performed 3-(4,5-dimethylthiazol-2-yl)-5-(3-carboxymethoxyphenyl)-2-(4-sulfophenyl)-2H-tetrazolium (MTS) assays for measuring cell viability/proliferation and lactate dehydrogenase (LDH) release assay for evaluating cell damage. As shown in Supplementary material online, *Figure S4A*, there were no significant changes in the values of MTS at OD450nm between Ad.Lcn10- and Ad.GFP-ECs under either basal conditions or stimulation with LPS or TNFα. The amount of LDH released from Ad.Lcn10- and Ad.GFP-ECs were very low and showed no difference between the two groups upon either LPS or TNFα insults (see Supplementary material online, *Figure S4B*). Hence, the incubation of Ad.Lcn10- or Ad.GFP-infected ECs with LPS (10 μg/mL) or TNFα (10 ng/mL) for 3 h do not alter cell viability or cause cell damage. Taken together, these gain-of-function data clearly demonstrate that the elevation of endothelial Lcn10 could provide protection against inflammation-induced hyper-permeability.

3.5 RNA-Sequencing and gene enrichment analysis of Lcn10-overexpressing ECs

To dissect the mechanism underlying how Lcn10 regulates endothelial permeability, we thus performed RNA-sequencing analysis of the gene expression profile in Ad.Lcn10-infected ECs and control Ad.GFP-cells. To fully capitalize the gene signature of the whole transcriptome, especially to capture lower amplitude signals (e.g. lower fold changes) from expression variation that would otherwise fall below the signal-to-noise significance cut-off, we first conducted unbiased GSEA using whole MCEC transcriptomes. At a conventional threshold of $P < 0.05$, 133 gene sets were enriched from Gene Ontology resource. Highly enriched (Enrichment score ≥ 1.1 and FDR < 0.25) pathways in Ad.Lcn10-cells were Actin Cytoskeleton Organization and Biogenesis (*Figure 5A*) and Apical Junction Complex (*Figure 5B*). Using Kyoto Encyclopedia of Genes and Genomes database (KEGG), we further identified that adherens junction pathway was also enriched in Ad.Lcn10-cells, when compared with control cells (*Figure 5C*). Differentially expressed genes between the two groups were listed in heatmaps (*Figure 5A–C*). Next, when cut-off the log2-fold change at ≥ 0.1 and ≤ -0.1, there were a total of 147 differentially expressed genes with 102 upregulated and 45 downregulated in Ad.Lcn10-cells, compared to Ad.GFP-cells (*Figure 5D* and see Supplementary material online, *Table S3*). Consistent with the above unbiased GSEA assay, gene ontology (GO) enrichment analysis results also revealed that elevation of Lcn10 in ECs greatly activated two major signalling pathways involved in the regulation of actin cytoskeleton (*Figure 5E*) and cell junction (*Figure 5F*). Among the upregulated genes in Ad.Lcn10-cells, 11 genes were directly associated with the regulation of actin cytoskeleton including *Ssh1*, *Pfn1*, *Actg1*, *Itga3*, *LRP2*, *Celsr1*, *Nid2*, *Dag1*, *Syne2*, *Marcks*, and *Plxna4* (*Figure 5E*), meanwhile 16 genes were directly associated with the cell junction pathways, such as *Flna*, *Lamc1*, *Actg1*, *Tln1*, *Col4a2*, *Thbs1*, *Igf1r*, *Itga3*, *Fbln5*, *Lpp*, *Tns1*, *Ptprf*, *Cgnl1*, *Gja*1, *Lpar1*, and *Gucy1a2* (*Figure 5F*). Majority of these upregulated genes were further validated in Ad-Lcn10 ECs, using RT-qPCR (*Figure 5G*). Lastly, we asked whether Lcn10-induced elevation of these cytoskeleton/cell junction-related genes was suppressed in Lcn10-KO ECs. Unexpectedly, only the expression of *Ssh1*, *LRP2*, *Pfn1*, *Marcks*, *Actg1*, *Flna*, and *Lpar1* was significantly downregulated in Lcn10-KO ECs, compared to WT-ECs, whereas

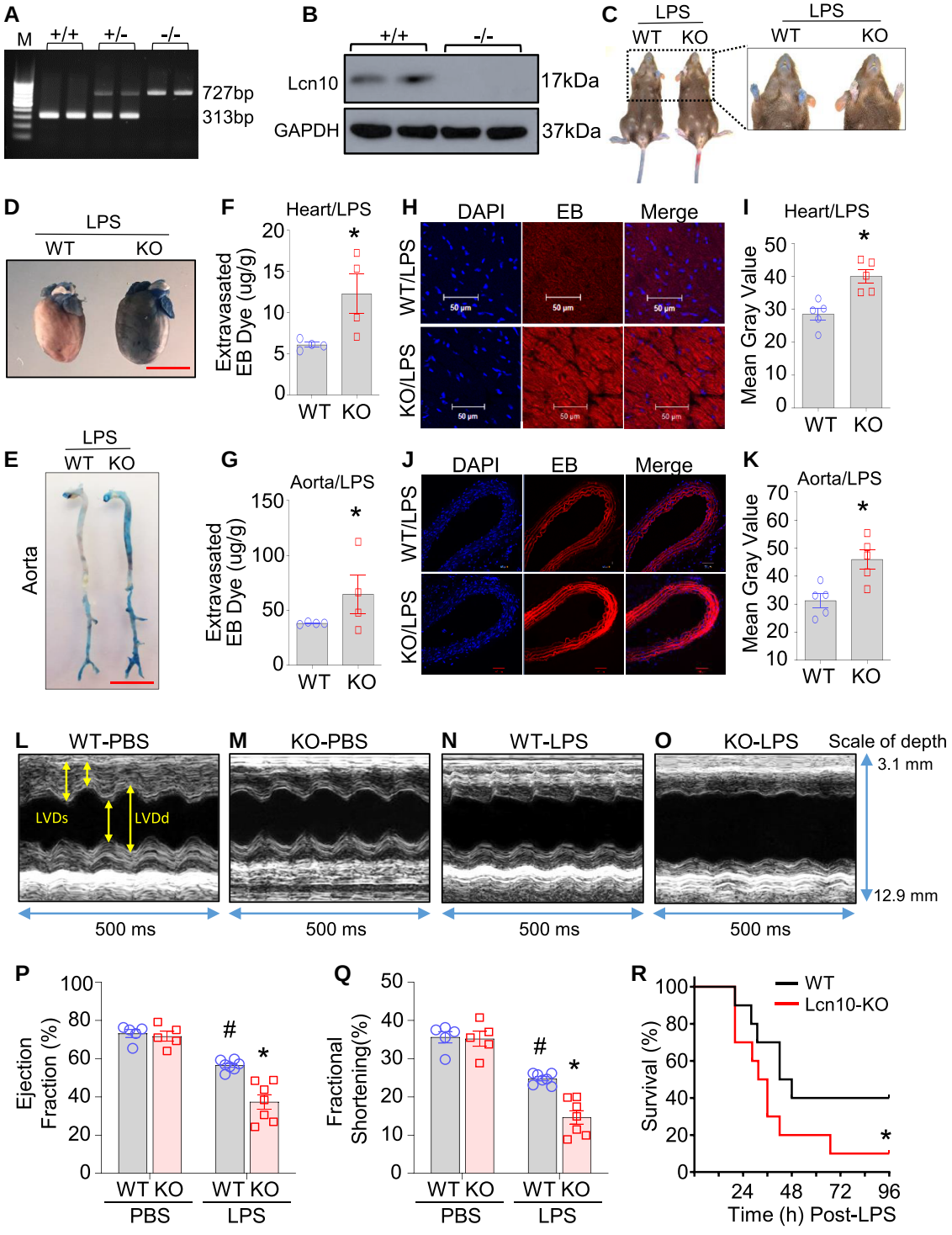

Figure 3 Lcn10 deficiency aggravates vascular leakage, organ injury, and mortality in mice upon systemic inflammatory conditions. (*A*) Genotyping analysis of $Lcn10^{+/+}$ (WT), $Lcn10^{+/-}$ (heterozygous), and $Lcn10^{-/-}$ (homozygous) mice. (*B*) Lcn10-KO mice were confirmed by Western blotting using heart tissue. (*C–K*) Lcn10-KO and WT mice were intraperitoneal injected with LPS (10 mg/kg BW). Twenty-hours later, the mice were intravenously injected with EB dye (4 mg/kg BW). The impaired peripheral circulation (*C*) and increased vascular leakage in the heart (*D*) and the aorta (*E*) were observed (scale bar: 5 mm). Vascular leakage in the heart (*F*) and the aorta (*G*) was analysed by incubating each heart in 500 μL formamide and each aorta in 200 μL formamide at 55°C for 48 h to elute EB dye for quantification ($n = 4$). Frozen sections of the heart (*H*) and the aorta (*J*) were observed for extravasated EB dye under a confocal microscope. Scale bar: 50μm. The intensity of relative red fluorescence within heart sections (*I*) and aorta sections (*K*) was quantified with Image J software ($n = 5$). (*L–Q*) 20 h after LPS or PBS injection, a cardiac function of Lcn10-KO and WT mice was measured by echocardiography. (*L–O*) Representative M-mode echocardiography recordings. (*P*) Left ventricular EF(%) and (*Q*) FS (%) were calculated ($n = 5–7$). Results of F, G, I, K, P, and Q are presented as mean ± SEM and analysed by student's *t*-test (*$P < 0.05$). (*R*) Kaplan–Meier survival curves were generated to compare mortality between two groups, significance was determined by log-rank (Mantel–Cox) test (*$P < 0.05$; $n = 20$ per group).

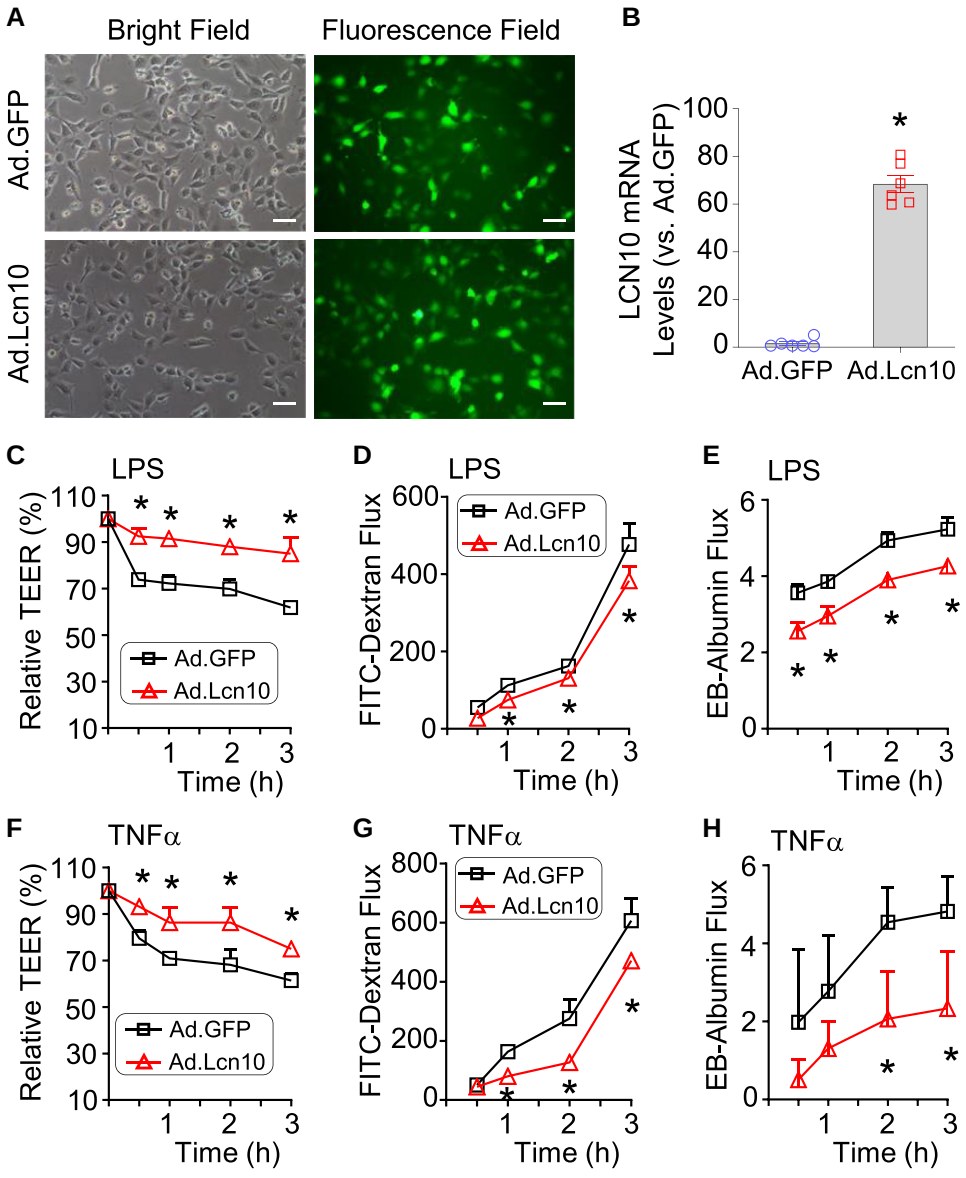

Figure 4 Overexpression of Lcn10 in MCECs attenuates inflammation-induced disruption of endothelial barrier integrity. (*A*) Adenoviral vector-mediated infection efficiency was evaluated by GFP expression at 24 h post-infection under a fluorescence microscope. Ad.Lcn10 vector contains an independent GFP-expression cassette in addition to Lcn10-cassette. Ad.GFP was used as control. Scale bar: 10 μm. (*B*) RT-qPCR analysis showed that Lcn10 was successfully overexpressed in Ad.Lcn10-infected ECs, when compared with Ad.GFP-cells ($n = 6$). Results are presented as mean ± SEM and analysed by student's *t*-test (*$P < 0.05$). (*C–E*) LPS-triggered EC monolayer leakage in Ad.Lcn10- and control Ad.GFP-cells were measured by (*C*) TEER, (*D*) FITC-dextran flux, and (*E*) EB-BSA flux. ($n = 4–6$). (*F–H*) Relative TEER values, FITC-dextran, and EB-BSA flux were determined in Ad.Lcn10-MCECs and control cells following TNFα challenge ($n = 4–6$). Results of (*C–H*) are presented as mean ± SD and analysed by two-way analysis of variance (ANOVA) (*$P < 0.05$).

loss of Lcn10 in ECs did not suppress but did activate expression of some genes including *Celsr1*, *Thbs1*, *Gucy1a2*, and *Lpp*, or did not affect expression of other genes including *Plxna4*, *Itga3*, *Lamc1*, *Col4a2*, *Gja1*, *Tln1*, and *Fbln5* (*Figure 5H*).

Of highest interest, Ssh1 was the most significantly upregulated gene in Lcn10-ECs (*Figure 5G*), whereas being greatly downregulated in Lcn10-KO ECs (*Figure 5H*). Importantly, Ssh1 is a well-known phosphatase that activates Cofilin, a key actin-binding protein that plays an essential role in modulating actin filament dynamics.[17] Based on the prior work on Ssh1 together with our bioinformatic analysis of RNA-seq data (*Figure 5A–F*), we, therefore, hypothesized that Lcn10-induced action on EC permeability during systemic inflammation is largely dependent on the Ssh1-Cofilin pathway.

3.6 Elevation of Lcn10 in ECs activates the Ssh1-Cofilin pathway, leading to reduced formation of stress fibres upon LPS insults

To test the above hypothesis (*Figure 6A*), we first determined whether Lcn10 could regulate Cofilin activation in ECs. Given that Ssh1 activates Cofilin by dephosphorylation at Ser-3,[17] we, therefore, measured Cofilin

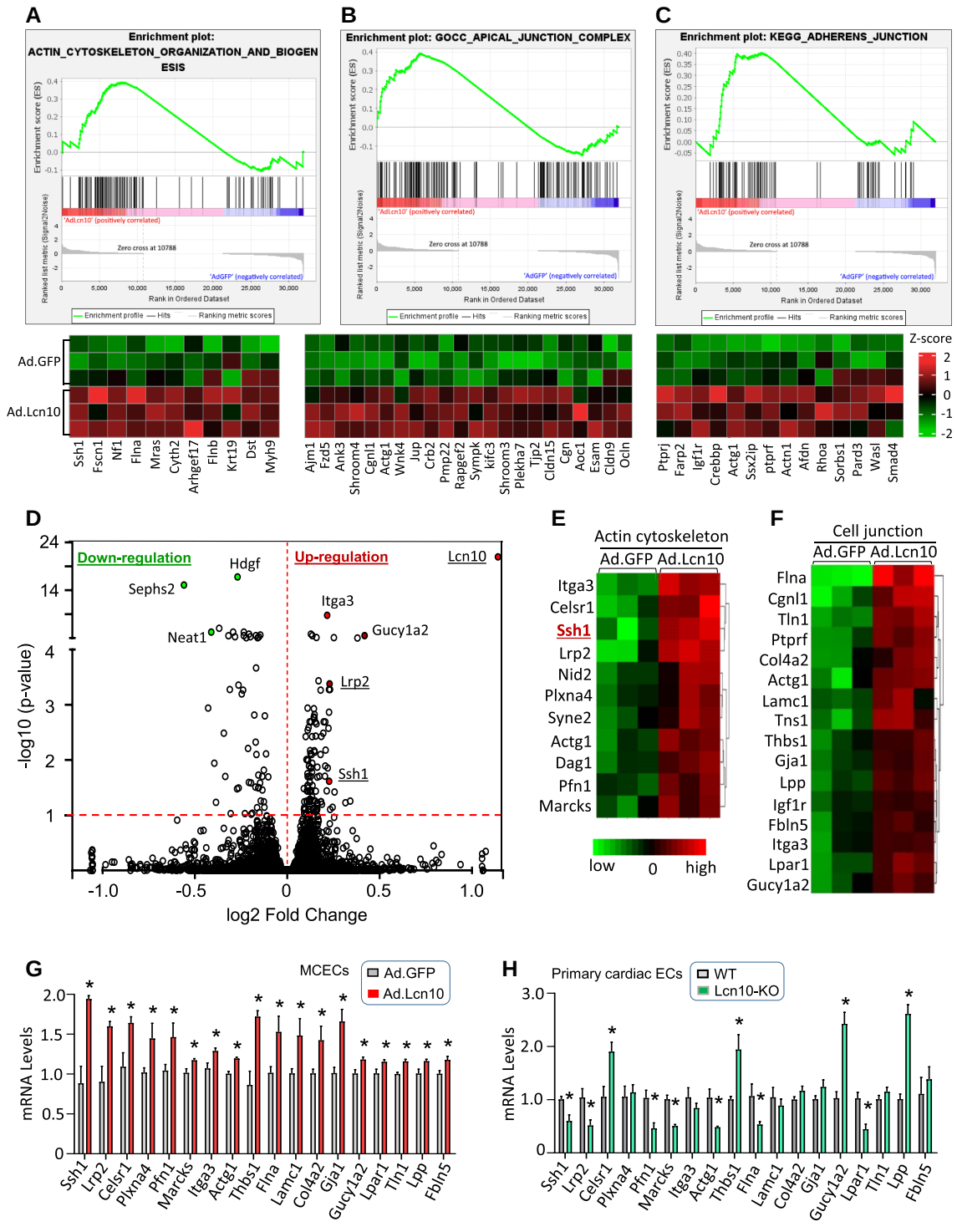

Figure 5 Gene expression profile analysis of Ad.Lcn10-infected MCECs and controls. (*A–C*) Enrichment plots from GSEA were used to identify the phenotypic change related to Lcn10 overexpression in MCECs. GSEA disclosed a significant enrichment of (*A*) actin cytoskeleton organization and biogenesis, (*B*) apical junction complex, and (*C*) Adherens junction. Heatmaps of differentially expressed genes were created, and highly differential gene sits are demonstrated. (*D*) Volcano plot of the overall gene expression alteration in Ad.Lcn10-ECs when compared with Ad.GFP-cells ($n = 3$ per group). (*E* and *F*) Heatmaps showing differentially expressed genes in Ad.Lcn10-ECs are involved in the regulation of (*E*) actin cytoskeleton and (*F*) cell junction pathway. (*G*) Eighteen of those upregulated genes that are associated with the actin cytoskeleton and cell junction pathway were validated in another batch of Ad.Lcn10- and Ad.GFP-infected cells using RT-qPCR ($n = 4–6$). (*H*) The expression levels of those 18 genes above were further examined in primary ECs isolated from Lcn10-KO and WT mice, using RT-qPCR ($n = 4$). All results are presented as mean ± SEM and analysed by student's *t*-test (*$P < 0.05$).

and its Ser-3-phosphorylated levels in Ad.Lcn10- and Ad.GFP-infected ECs by Western-blotting. We observed that Ad.Lcn10-ECs had higher levels of Ssh1 than Ad.GFP-cells (*Figure 6B*), consistent with our RNA-seq data above. Accordingly, the phosphorylated levels of Cofilin and its ratio to total Cofilin protein were significantly lower in Ad.Lcn10-cells than in Ad.GFP-cells (*Figure 6B*), suggesting its dephosphorylation and activation by Ssh1. Given that Cofilin is well-characterized to control actin filament re-organization by stimulating the severance and depolymerization of actin filaments[17] (*Figure 6A*), we next examined cytoskeletal structures (i.e. stress fibres and cortical actin networks), using Alexa-Fluor 594 phalloidin (F-actin probe) staining. As shown in *Figure 6C* (white arrows) and Supplementary material online, *Figure S5A*, under basal conditions, GFP-ECs had a predominant cortical organization of F-actin along the cell periphery. After LPS stimulation, peripherally located F-actin was remodelled into centralized and irregular stress fibres running throughout the cytoplasm (*Figure 6C*, blue arrows). However, overexpression of Lcn10 strongly reinforced peripheral actin bands, both in unstimulated and LPS-treated cells (*Figure 6C*, white arrows). Importantly, the LPS-triggered formation of stress fibres was less pronounced in Lcn10-cells than in control GFP-cells (*Figure 6C*, blue arrows). Considering re-organization of the actin cytoskeleton affects the stability of EC junctions and paracellular gap formation,[9–11,17] we then evaluated the integrity of cell peripheral membrane by staining these ECs with an antibody to ZO-1, a tight junction protein. As shown in *Figure 6D* and Supplementary material online, *Figure S5B*, the linear shape of cell-cell junctions was displayed in both GFP- and Lcn10-cells under basal conditions. However, LPS treatment greatly disrupted the integrity of cell junctions, as evidenced by much more jagged and disconnected ZO-1 staining in GFP-cells, but less in Lcn10-cells (*Figure 6D*, yellow arrows). Together, these data indicate that forced elevation of Lcn10 in ECs activates the Ssh1-Cofilin pathway and reinforces the cortical actin filament upon LPS insult, leading to reduced stress fibre formation and repressed opening of cell junctions.

3.7 Knockdown of Ssh1 in ECs suppresses Lcn10-induced reduction of permeability upon inflammatory conditions

To test whether Lcn10-elicited reduction of endothelial leakage during systemic inflammation is dependent on Ssh1 signalling, we utilized sequence-specific siRNA to knockdown Ssh1 expression in Ad.Lcn10-infected ECs, followed by LPS challenge for EC permeability analysis. Western-blotting data revealed that the elevation of Ssh1 in Ad.Lcn10-ECs was greatly reduced by siRNA-Ssh1 (si-Ssh1) to a similar level as in GFP-cells (*Figure 6E*). Consequently, Lcn10-induced suppression of Cofilin activity was greatly blocked by siRNA-Ssh1 transfection, as revealed by similar degree of Cofilin phosphorylation and its ratio to total Cofilin protein between siRNA-Ssh1/Ad.Lcn10-ECs and control siRNA-Ssh1/Ad.GFP-cells (*Figure 6E*). Endothelial leakage analysis, measured with TEER value, FITC-dextran, and EB-BSA fluxes, further indicated that the drops of TEER values, fluxes of FITC-dextran, and EB-albumin were greatly reduced in Lcn10-cells, compared to GFP-cells following LPS challenge (*Figure 6F–H*, see Supplementary material online, *Figure S6A–C*). However, such inflammation-caused leakage was significantly increased in Lcn10-cells when the expression of Ssh1 was silenced by siRNAs (*Figure 6F–H*, see Supplementary material online, *Figure S6A–C*). Taken together, these data indicate that knockdown of Ssh1 by siRNA inhibits the Lcn10-induced dephosphorylation of Cofilin (activation) and accordingly, disrupts Lcn10-elicited EC integrity upon inflammatory conditions (*Figure 6I*). It suggests that Lcn10-mediated endothelial protection against inflammation-triggered leakage is largely dependent on the Ssh1-Cofilin signalling.

3.8 Lcn10 regulates Ssh1 expression in ECs *via* LRP2

To identify possible mediators for the Lcn10-induced upregulation of Ssh1 in ECs, we next analysed our RNA expression profiles in Ad.Lcn10-ECs for searching membrane receptors as candidates, because Lcn10 is a secreted protein and prior work has shown that LCN family members interact with LDL receptor-related proteins (LRPs).[45] Interestingly, our above RNA-seq data (*Figure 5*) reveal that the expression of LRP2 was significantly elevated in Lcn10-ECs compared to control GFP-cells. As a matter of fact, the online LRP2-protein interaction network database (https://bioinfo.uth.edu/ccmGDB/) also demonstrates that LRP2 could interact with Lcn10 in UCECs (uterine corpus endometrial carcinoma cells) (see Supplementary material online, *Figure S7A*). Using co-immunostaining of ECs with anti-LRP2 and anti-Lcn10 antibodies, we did observe partially co-localization of LRP2 with Lcn10 on the surface of ECs (*Figure 7A*). Furthermore, we performed protein–protein binding ELISA assays (*Figure 7B*) and observed that recombinant LRP2-protein (rLRP2)-coated wells, but not BSA-coated wells, captured recombinant Lcn10 protein (rLcn10) dose-dependently (*Figure 7C*). Similarly, rLcn10-coated wells could bind rLRP2-protein dose-dependently, compared to BSA-coated controls (*Figure 7D*). These data indicate that Lcn10 may directly interact with LRP2. More interestingly, we found that the addition of rLcn10 (200 ng/mL) to cultured ECs promoted the expression of both LRP2 and Ssh1, compared to BSA-controls (*Figure 7E*). However, when LRP2 was knocked down by siRNA (si-LRP2), rLcn10-mediated upregulation of Ssh1 expression was counteracted (*Figure 7F*). Consistently, the elevation of Ssh1 in Ad.Lcn10-infected ECs were also blocked by siRNA-LRP2 (*Figure 7G*). These data suggest that there may be a positive feedback loop involving Lcn10-LRP2-Ssh1, and Lcn10 upregulates Ssh1 expression in ECs through its interaction with LRP2.

Along this line, we then asked whether the exogenous addition of rLcn10 to ECs could reduce LPS-triggered hyper-permeability and if so, whether the LRP2-Ssh1 signalling was involved. To address these questions, we treated these cells with rLcn10 protein or control BSA for 12 h, followed by the addition of LPS (10 μg/mL) for barrier integrity and permeability assays. Please note that endotoxin levels in rLcn10 and BSA proteins are <0.01EU/μg, low enough to exclude its effects. We observed that treatment with rLcn10 greatly blunted LPS-induced decreases of TEER values in a time-dependent manner, compared to control BSA-treated cells after LPS insult (*Figure 7H*). Similarly, the leakage of FITC-dextran (see Supplementary material online, *Figure S7B*) and EB-albumin (see Supplementary material online, *Figure S7C*) was significantly inhibited in rLcn10-ECs, compared to BSA-cells following the LPS challenge.

Importantly, when LRP2 was knocked down by siRNAs in ECs, rLcn10-induced attenuation of TEER drops was significantly offset, as evidenced by similar decreases of TEER values between BSA- and rLcn10-treated cells at 2 h post-CLP challenge (*Figure 7I*). Likewise, pre-knockdown of Ssh1 in rLcn10-treated ECs displayed no protection against LPS-induced endothelial leakage, as no differences in relative TEER values between two groups (*Figure 7J*). Of interest, we noticed that knockdown of LRP2, albeit offset rLcn10-provided protection, did not affect endothelial permeability during inflammation (*Figure 7I*). This may be ascribed to its functionally complex as it is a huge protein with molecular weight (MW) ≈600 kDa and binds at least 30 different ligands with each interaction activating distinct cellular signalling cascades.[46] In this regard, Ssh1 is just one of its downstream signalling activated by Lcn10 in ECs.

To further determine whether rLcn10-mediated protection against EC monolayer leakage is associated with Ssh1-controlled actin re-arrangement, we performed immunostaining with Alexa Fluor 488 phalloidin for actin filament analysis in rLcn10-treated ECs and control cells at 2 h post-LPS insults. We found that in control BSA-cells after LPS stimulation, peripherally located F-actin was re-organized into stress-fibre bundles, spreading across the cytoplasm (see Supplementary material online, *Figure S7D*). However, treatment with rLcn10 strongly reinforced peripheral actin (cortical actin) bands and inhibited stress-fibre formation upon LPS challenge (see Supplementary material online, *Figure S7D*).

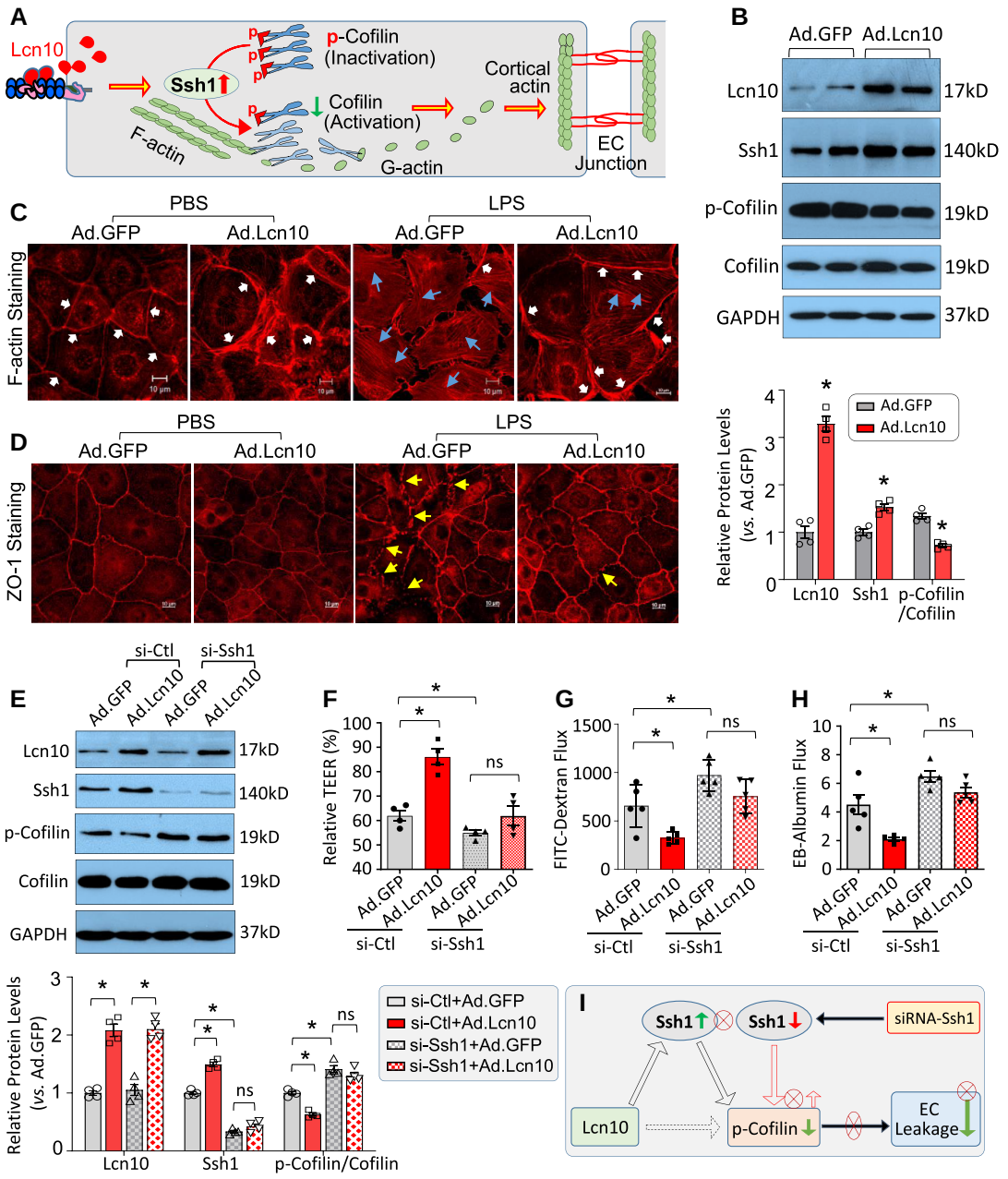

Figure 6 Overexpression of Lcn10 in ECs activates Ssh1/Cofilin-mediated actin re-arrangement, whereas knockdown of Ssh1 in ECs suppresses Lcn10-induced reduction of endothelial permeability upon LPS insults. (*A*) Cartoon scheme depicting how Lcn10 regulates Ssh1/Cofilin-mediated actin turnover from stress fibre (F-actin) to cortical actin in ECs. Lcn10-caused elevation of Ssh1 promotes more dephosphorylation of Cofilin which activates more depolymerization of stress fibre F-actin to new G-actin monomers for the formation of cortical actin to anchor junction molecules between ECs and reduces EC leakage. (*B*) Representative immuno-blots and their quantification results for the protein levels of Lcn10, Ssh1, *p*-Cofilin, and total Cofilin as well as the ratio of *p*-Cofilin to total Cofilin in Ad.Lcn10- and Ad.GFP-ECs. Glyceraldehyde-3-phosphate dehydrogenase (GAPDH) was used as a loading control (*$P < 0.05$, $n = 4$). (*C*) Representative confocal images of immunostaining with Alexa-Fluor 594 phalloidin (F-actin probe) to determine the formation of the cortical actin filament (white arrows) and stress fibres (blue arrows) in Ad.Lcn10- and Ad.GFP-ECs at 2 h post-LPS challenge. (*D*) Immunostaining analysis of EC membrane integrity in Ad.Lcn10- and Ad.GFP-ECs at 2 h post-LPS challenge using Alexa-Fluor 594 conjugated ZO-1 antibody. Yellow arrows indicate the disrupted peripheral membrane. Treatment of ECs with PBS was used as a basal condition (Scale bar, 10 μm). (*E*) Representative immuno-blots and their quantification analysis of the Lcn10-Ssh1-Cofilin cascades in MCECs pre-transfected with siRNA-Ssh1 (si-Ssh1) and control siRNA (si-Ctl) for 48 h, followed by infection with Ad.Lcn10 or Ad.GFP for 24 h. GAPDH was used as a loading control. ($n = 4$); ns: not significant. (*F–H*) In parallel, these MCECs pre-transfected with siRNAs, followed by infection with Ad.Lcn10 or Ad.GFP as above were subjected to LPS insults for 2 h, and then EC monolayer permeability was determined by measuring (*F*) TEER, (*G*) FITC-dextran flux, and (*H*) EB-Albumin flux ($n = 4–5$). All results are presented as mean ± SEM and analysed by student's *t*-test (*$P < 0.05$). (*I*) Cartoon scheme summarizing that siRNA-mediated knockdown of Ssh1 offsets Lcn10-elicited effects on dephosphorylation of Cofilin and EC integrity.

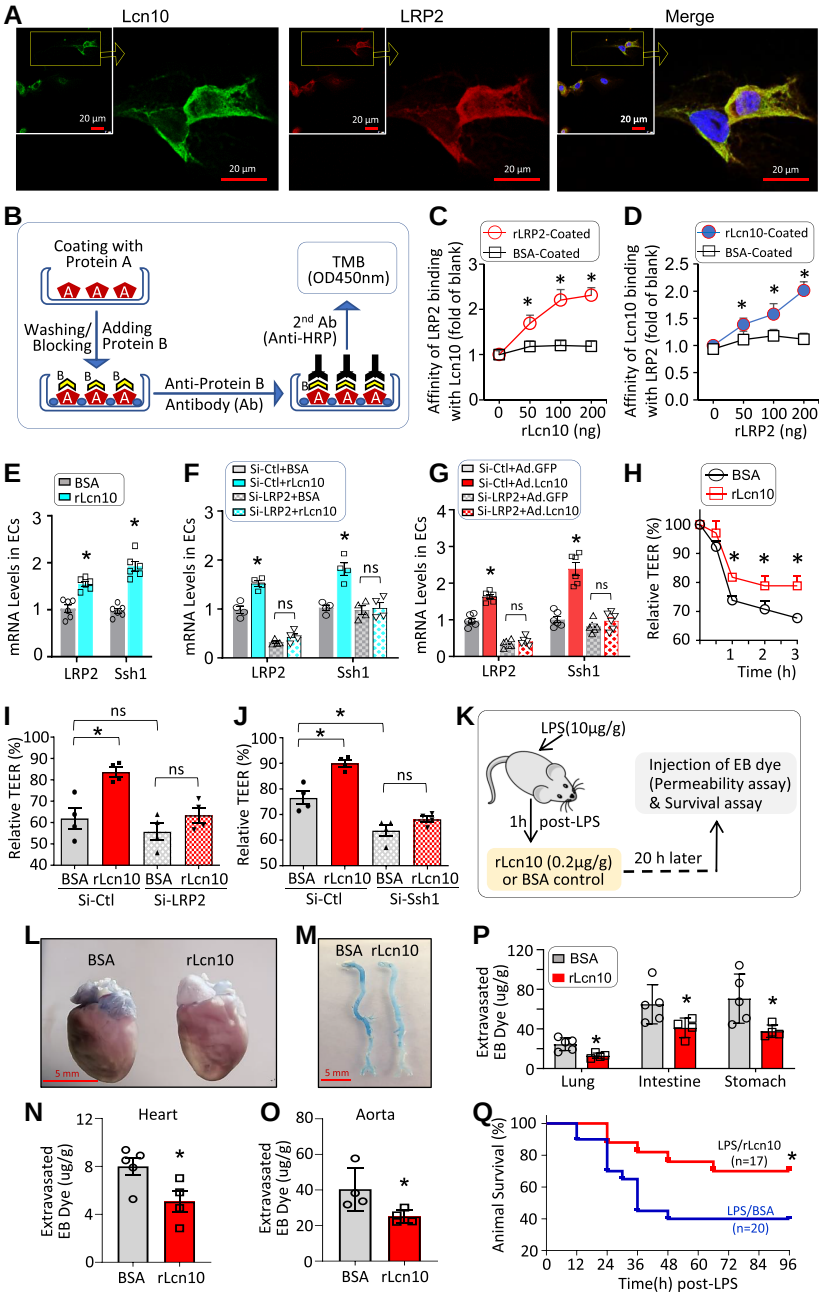

Figure 7 Lcn10 interacts with LRP2 receptor and recombinant Lcn10 protein (rLcn10) protects against inflammation-triggered EC leakage *in vitro* and *in vivo*. (*A*) Representative image of co-immunofluorescence staining for Lcn10 (green) and LRP2 (red) in MCECs [blue, 4',6-diamidino-2-phenylindole (DAPI) for nuclei]. Yellow frame inserts are zoomed out. The red scale bar: 20 μm. (*B*) A diagram for experimental procedures of protein–protein binding ELISA analysis to measure the affinity of protein A binding with protein B. (*C*) Recombinant LRP2-protein (rLRP2) pre-coated on a high-binding ELISA plate dose-dependently captured the Lcn10 protein (rLcn10), whereas BSA-coated wells did not arrest the Lcn10 protein ($n = 4$). (*D*) Recombinant Lcn10 protein-coated wells, but not BSA-coated ones, could does-dependently capture LRP2-protein ($n = 4$). (*E*) Exogenous addition of rLcn10 to ECs could upregulate both LRP2 and Ssh1 expression, measured by RT-qPCR ($n = 4$–6). (*F* and *G*) RT-qPCR analysis shows that knockdown of LRP2 by siRNA (si-LRP2) blocks Lcn10-induced elevation of Ssh1 in both (*F*) rLcn10-treated ECs and (*G*) Ad.Lcn10-ECs, compared to respective controls ($n = 4$–6; ns: not significant). (*H*) Treatment of ECs with rLcn10 (200 ng/mL) blunts the LPS-caused drops in TEER, compared to BSA-controls ($n = 4$). (*I*) Knockdown of LRP2 by siRNA (si-LRP2) and (*J*) knockdown of Ssh1 by siRNA (si-Ssh1) both greatly offset rLcn10-induced elevation of TEER ($n = 4$; ns, not significant). (*K*) WT mice were intraperitoneal injected with LPS (10 μg/g BW). One hour later, rLcn10 (0.2 μg/g BW) or BSA (control) was injected *via* the tail vein. After 20 h, mice were intravenously infused with EB dye (4 μg/g BW). Vascular leakage within (L/*N*) the heart, (M/O) the aorta, and (*P*) the lung, intestine, and stomach were analysed in rLcn10- and BSA-treated group ($n = 4$–5). Scale bars for L/M: 5 mm. Results of C, D, and H are presented as mean ± SD and analysed by two-way analysis of variance (ANOVA) (*$P < 0.05$). Results of E-G, I, J, and *N-P* are presented as mean ± SEM and analysed by student's *t*-test (*$P < 0.05$). (*Q*) The mortality of LPS-mice was monitored after the treatment with rLcn10 or BSA control. $n = 20$ for BSA-treated group, $n = 17$ for rLcn10-treated group. Kaplan–Meier survival curves were generated to compare mortality between two groups, and significance was determined by log-rank (Mantel–Cox) test (*$P < 0.05$).

Furthermore, when expression of Ssh1 was pre-knocked down by siRNAs (si-Ssh1), rLcn10-induced beneficial effects on actin filament re-organization were blocked, as evidenced by a similar degree of stress fibre and cortical actin filament between rLcn10-treated ECs and BSA-controls (see Supplementary material online, *Figure S7E*).

Put together, our data presented here suggest that endogenous elevation of Lcn10 can be secreted outside ECs and elicits autocrine function to interact with LRP2, leading to the activation of Ssh1-Confilin pathway and consequently, promoting the assembly of cortical actin filaments and thereby, inhibiting inflammation-triggered vascular leakage (See graphic abstract).

3.9 Therapeutic effects of rLcn10 protein in inflammation-triggered vascular leakage

To further test whether recombinant Lcn10 protein (rLcn10) has potential therapeutic effects *in vivo*, we injected (*i.p.*) LPS into WT mice, followed by injection of rLcn10 (0.2 μg/g) or BSA control *via* the tail vein (*Figure 7K*). At 20 h post-LPS challenge, EB dye was infused through the tail vein to measure vascular permeability in the heart, aorta, lung, intestine, and stomach (*Figure 7K*). Excitingly, we observed that EB extravasation in the heart (*Figure 7L*) and the aorta (*Figure 7M*) was reduced to a greater degree in rLcn10-treated endotoxic mice when compared to BSA-treated controls, as quantified by elution of EB dye into formamide solution (*Figure 7N* and *O*). In addition, rLcn10-mediated reduction of EB leakage during endotoxemia was also detected in the lung, intestine, and stomach (*Figure 7P*). Given that treatment of endotoxic mice with rLcn10 mitigates vascular permeability, we next used another two batches of WT mice following the same experimental procedure (*Figure 7K*) to monitor animal mortality over the course of 4 days. We observed that the survival rate was significantly improved in LPS-mice treated with rLcn10, as evidenced by 71% of the mice ($n = 17$) survived until the end of day 4, when only 40% of BSA-treated mice survived ($n = 20$) (*Figure 7Q*). Collectively, these translational data suggest that injection of rLcn10 into systemic inflammatory mice could reduce vascular leakage, leading to enhanced animal survival.

4. Discussion

In this study, for the first time, we demonstrate that the expression of cardiac Lcn10 is transiently increased and then greatly reduced only in ECs, but not in either fibroblasts or cardiomyocytes in response to inflammatory stimuli. Using *in vitro* cultured mouse cardiac endothelial cells (MCECs) and a global Lcn10-KO mouse model, we uncovered that loss of Lcn10 caused endothelial hyper-permeability, multiple organ injury, and cardiac dysfunction upon inflammatory challenge. By contrast, both endogenous and exogenous elevation of Lcn10 significantly restrained inflammation-induced endothelial monolayer leakage. Mechanistically, we identified that Lcn10 interacts with the LRP2 receptor and consequently, activates its downstream Ssh1-Cofilin signalling cascade, leading to the promotion of actin filament re-arrangement to cortical actin and the maintenance of endothelial barrier integrity. Translationally, injection of recombinant Lcn10 protein could have therapeutic effects against inflammation-triggered vascular leakage.

It is currently recognized that the regulation of vascular permeability is mediated by two main mechanisms, transcellular pathway and paracellular pathway.[47,48] The transcellular pathway is that substances are mostly forced to pass through ECs while passing between the cells is paracellular pathway.[47,48] Measurements of TEER and macromolecular permeability are known to reflect different aspects of EC barrier function which may be differentially regulated under various inflammatory conditions.[38] TEER is an indicator of the overall integrity of the endothelial barrier, whereas the flux of macromolecules such as FITC-dextran and EB-BSA is more related to a paracellular pathway.[38] Our data presented in this study are consistent between TEER and macromolecular flux measurements, suggesting that Lcn10-mediated reduction of endothelial permeability is through the maintenance of paracellular integrity.

Previous studies have shown that major molecules involved in the paracellular pathway are tight junctions (TJs) and adhesion junctions (AJs).[47–49] The former group includes transmembrane proteins (i.e. occludin and claudin) and cytoplasmic scaffolding proteins (i.e. ZO-1, -2, and -3).[49] The latter has consisted of transmembrane protein (i.e. VE-cadherin) and intracellular components (i.e. p120-catenin, β-catenin, and α-catenin).[49] In this study, we also measured the expression levels of ZO-1, VE-Cadherin, and occluding in Ad-Lcn10-ECs, however, which showed no differences in comparison with control Ad.GFP-cells (see Supplementary material online, *Figure S8*). Interestingly, our immuno-staining results showed more continuous ZO-1 band on the Lcn10-ECs. This suggests that the elevation of Lcn10 might promote ZO-1 stability. Indeed, the stabilization of EC junction protein and formation of paracellular gap is influenced by re-arrangement of the actin cytoskeleton. More stress-fibre formation in ECs could produce a stronger concentric pulling force to form a paracellular gap, whereas more generation of peripheral actin band provides a stronger edge base to anchor/stabilize junction proteins. Our data presented in this study clearly demonstrates the reduced formation of stress fibre and increased generation of cortical actin bands in both Ad.Lcn10-infected (*Figure 6C*) and rLcn10-treated ECs (see Supplementary material online, *Figure S7D*). Therefore, Lcn10-mediated protection of endothelial barrier integrity upon inflammatory conditions is largely ascribed to actin filament re-organization.

Regarding endothelial actin re-arrangement in response to inflammatory stimulation, previous work has shown that Slingshot-1 (Ssh1), a member of a dual-specificity protein phosphatase family, regulates actin dynamics by dephosphorylating and reactivating Cofilin, an actin-depolymerizing factor.[17] Phosphorylation of Cofilin is mediated by LIM kinases (LIMK) and dephosphorylation by Slingshot phosphatases.[17] At present, upstream regulators of the LIMK-Cofilin signalling cascade have been well-characterized in ECs.[16,17] Nonetheless, how to modulate endothelial Ssh1-Cofilin pathway is less well investigated. Our study presented here reveals that Lcn10 positively regulates endothelial Ssh1 expression through its interaction with the LRP2 receptor and consequently, Lcn10-induced action on endothelial actin turnover is largely dependent on Ssh1. In addition, our RNA-seq data and RT-qPCR analysis (see Supplementary material online, *Figure S8*) also showed no any changes in the expression of LIMKs in Ad.Lcn10-ECs, compared to controls, which excludes the possibility of LIMKs' contribution to the Lcn10-mediated protection.

There are several limitations to this study. First, it remains unclear how the interaction of Lcn10 with LRP2 activates Shs1 expression in ECs. LRP2 is a large transmembrane receptor expressed on absorptive epithelia and ECs where it binds dozens of extracellular ligands to control distinctive signalling pathways and plays versatile functions.[46] Similar to our present findings, one recent study by Woo *et al.* showed that endogenously overexpression of RanBP9 in neuron cells could bind to the LRP2 receptor and up-regulated Ssh1 expression, but its underlying mechanism remains obscure.[50] Future experimental work needs to dissect how LRP2 regulates Ssh1 expression and actin dynamics. Second, we utilized a global Lcn10-KO mouse model instead of tissue-specific KO mice. Considering Lcn10 is a secreted protein that may have paracrine effects,[18] endothelial Lcn10-specific KO mouse model is unlikely to provide clear and accurate results for discerning the role of Lcn10 in inflammation-caused vascular leakage. Finally, one would argue that cardiac Lcn10 levels are increased during the early phase of inflammatory conditions, why recombinant Lcn10 protein has therapeutic effects? Indeed, this early elevation of cardiac Lcn10 in response to inflammation should be a compensatory protective mechanism. We also measured Lcn10 levels in whole blood cells upon inflammatory conditions and found that the expression of Lcn10 was remarkably decreased, compared to controls following either LPS injection or CLP surgery (see Supplementary material online, *Figure S9A and B*), which is consistent with reduced serum Lcn10 level in human patients with severe sepsis.[28]

In conclusion, this study provides the first evidence showing that endothelial Lcn10 is essential for protecting against massive inflammation-triggered vascular leakage. We identify the Lcn10-LRP2-Ssh1 axis as a new link to the regulation of endothelial barrier integrity. These findings presented in this work greatly advance our knowledge of the mechanism

of vascular leakage that occurs during systemic inflammation. Most importantly, our data clearly define Lcn10 as a new regulator of EC function and as a potential therapeutic agent for the treatment of inflammation-induced vascular hyper-permeability.

Supplementary material

Supplementary material is available at *Cardiovascular Research* online.

Author contributions

H.Z. and P.W. designed and performed experiments, analysed data, and wrote the manuscript. X.W. and W.H. helped to perform transthoracic echocardiography and analysed the result. H.-H.Y. and Y.Y.L. performed experiments and analysed data. W.D., J.C., and Y.F. helped with bioinformatic analysis of RNA-seq data. T.P., C.G., Y.W. S.S., C.M., and C.W. helped with experimental design, data analysis and critically reviewed the manuscript. G.-C.F. analysed results, reviewed/edited manuscript, provided financial and administrative support, and gave final approval of the manuscript.

Acknowledgements

This study was supported by National Institutes of Health (NIH) grants R01 (GM-132149, GM-149538, and HL-160811 to G.-C. Fan). Y.W. has received support from NIH grants (HL157456 and HL143490). Sadayappan has received support from National Institutes of Health grants R01 AR078001, R01 HL130356, R01 HL105826, R38 HL155775, and R01 HL143490, the American Heart Association 2019 Institutional Undergraduate Student (19UFEL34380251) and Transformation (19TPA34830084) awards, the PLN Foundation (PLN crazy idea) and the Leducq Foundation (Transatlantic Network 18CVD01, PLN-CURE).

Conflict of interest: Dr. Sadayappan provides consulting and collaborative research studies to the Leducq Foundation (CURE-PLAN), Red Saree Inc., Greater Cincinnati Tamil Sangam, Novo Nordisk, Pfizer, AavantioBio, AstraZeneca, MyoKardia, Merck, and Amgen, but such work is unrelated to the content of this article.

Data availability

Data supporting the findings of this study are available upon reasonable request to the corresponding author.

References

1. Rossaint J, Zarbock A. Pathogenesis of multiple organ failure in sepsis. *Crit Rev Immunol* 2015;**35**:277–291.
2. Faist A, Janowski J, Kumar S, Hinse S, Çalışkan DM, Lange J, Ludwig S, Brunotte L. Virus infection and systemic inflammation: lessons learnt from COVID-19 and beyond. *Cells* 2022;**11**:2198.
3. Ciutac AM, Dawson D. The role of inflammation in stress cardiomyopathy. *Trends Cardiovasc Med* 2021;**31**:225–230.
4. Pons S, Fodil S, Azoulay E, Zafrani L. The vascular endothelium: the cornerstone of organ dysfunction in severe SARS-CoV-2 infection. *Crit Care* 2020;**24**:353.
5. Hellenthal KEM, Brabenec L, Wagner NM. Regulation and dysregulation of endothelial permeability during systemic inflammation. *Cells* 2022;**11**:1935.
6. Tiwari A, Elgrably B, Saar G, Vandoorne K. Multi-scale imaging of vascular pathologies in cardiovascular disease. *Front Med* 2022;**8**:754369.
7. Dolmatova EV, Wang K, Mandavilli R, Griendling KK. The effects of sepsis on endothelium and clinical implications. *Cardiovasc Res* 2021;**117**:60–73.
8. Yang Q, Wijerathne H, Langston JC, Kiani MF, Kilpatrick LE. Emerging approaches to understanding microvascular endothelial heterogeneity: a roadmap for developing anti-inflammatory therapeutics. *Int J Mol Sci* 2021;**22**:7770.
9. García-Ponce A, Citalán-Madrid AF, Velázquez-Avila M, Vargas-Robles H, Schnoor M. The role of actin-binding proteins in the control of endothelial barrier integrity. *Thromb Haemost* 2015;**113**:20–36.
10. Schnoor M, García Ponce A, Vadillo E, Pelayo R, Rossaint J, Zarbock A. Actin dynamics in the regulation of endothelial barrier functions and neutrophil recruitment during endotoxemia and sepsis. *Cell Mol Life Sci.* 2017;**74**:1985–1997.
11. Rho SS, Ando K, Fukuhara S. Dynamic regulation of vascular permeability by vascular endothelial cadherin-mediated endothelial cell-cell junctions. *J Nippon Med Sch* 2017;**84**:148–159.
12. Rigor RR, Shen Q, Pivetti CD, Wu MH, Yuan SY. Myosin light chain kinase signaling in endothelial barrier dysfunction. *Med Res Rev* 2013;**33**:911–933.
13. van Buul JD, Timmerman I. Small rho GTPase-mediated actin dynamics at endothelial adherens junctions. *Small GTPases* 2016;**7**:21–31.
14. Barlow HR, Cleaver O. Building blood vessels-one rho GTPase at a time. *Cells* 2019;**8**:545.
15. Ohashi K. Roles of cofilin in development and its mechanisms of regulation. *Dev Growth Differ* 2015;**57**:275–290.
16. Berabez R, Routier S, Bénédetti H, Plé K, Vallée B. LIM kinases, promising but reluctant therapeutic targets: chemistry and preclinical validation in vivo. *Cells* 2022;**11**:2090.
17. Mizuno K. Signaling mechanisms and functional roles of cofilin phosphorylation and dephosphorylation. *Cell Signal* 2013;**25**:457–469.
18. Charkoftaki G, Wang Y, McAndrews M. Update on the human and mouse lipocalin (LCN) gene family, including evidence the mouse mup cluster is result of an "evolutionary bloom". *Hum Genomics* 2019;**13**:11.
19. Bergwik J, Kristiansson A, Allhorn M, Gram M, Åkerström B. Structure, functions, and physiological roles of the lipocalin α_1-microglobulin (A1M). *Front Physiol* 2021;**12**:645650.
20. Christoffersen C. Apolipoprotein M-A marker or an active player in type II diabetes? *Front Endocrinol* 2021;**12**:665393.
21. Chen JJ, Lee TH, Lee CC, Chang CH. Using lipocalin as a prognostic biomarker in acute kidney injury. *Expert Rev Mol Diagn* 2021;**21**:455–464.
22. Mondal A, Bose D, Saha P, Sarkar S, Seth R, Kimono D, Albadrani M, Nagarkatti M, Nagarkatti P, Chatterjee S. Lipocalin 2 induces neuroinflammation and blood-brain barrier dysfunction through liver-brain axis in murine model of nonalcoholic steatohepatitis. *J Neuroinflammation* 2020;**17**:201.
23. Christensen PM, Liu CH, Swendeman SL, Obinata H, Qvortrup K, Nielsen LB, Hla T, Di Lorenzo A, Christoffersen C. Impaired endothelial barrier function in apolipoprotein M-deficient mice is dependent on sphingosine-1-phosphate receptor 1. *FASEB J* 2016;**30**:2351–2359.
24. Mathiesen Janiurek M, Soylu-Kucharz R, Christoffersen C, Kucharz K, Lauritzen M. Apolipoprotein M-bound sphingosine-1-phosphate regulates blood-brain barrier paracellular permeability and transcytosis. *Elife* 2019;**8**:e49405.
25. Yao Mattisson I, Christoffersen C. Apolipoprotein M and its impact on endothelial dysfunction and inflammation in the cardiovascular system. *Atherosclerosis* 2021;**334**:76–84.
26. di Salvo TG, Yang KC, Brittain E, Absi T, Maltais S, Hemnes A. Right ventricular myocardial biomarkers in human heart failure. *J Card Fail* 2015;**21**:398–411.
27. Wang L, Xie W, Li G, Hu B, Wu W, Zhan L, Zou H. Lipocalin 10 as a new prognostic biomarker in sepsis-induced myocardial dysfunction and mortality: a pilot study. *Mediators Inflamm.* 2021;**2021**:6616270.
28. Tsalik EL, Langley RJ, Dinwiddie DL, Miller NA, Yoo B, van Velkinburgh JC, Smith LD, Thiffault I, Jaehne AK, Valente AM, Henao R, Yuan X, Glickman SW, Rice BJ, McClain MT, Carin L, Corey GR, Ginsburg GS, Cairns CB, Otero RM, Fowler VG, Rivers EP, Woods CW, Kingsmore SF. An integrated transcriptome and expressed variant analysis of sepsis survival and death. *Genome Med* 2014;**6**:111.
29. Yndestad A, Landrø L, Ueland T, Dahl CP, Flo TH, Vinge LE, Espevik T, Frøland SS, Husberg C, Christensen G, Christensen G, Dickstein K, Kjekshus J, Oie E, Gullestad L, Aukrust P. Increased systemic and myocardial expression of neutrophil gelatinase-associated lipocalin in clinical and experimental heart failure. *Eur Heart J* 2009;**30**:1229–1236.
30. Alimadadi A, Munroe PB, Joe B, Cheng X. Meta-Analysis of dilated cardiomyopathy using cardiac RNA-Seq transcriptomic datasets. *Genes (Basel)*. 2020;**11**:60.
31. Li Q, Li Y, Huang W, Wang X, Liu Z, Chen J, Fan Y, Peng T, Sadayappan S, Wang Y, Fan GC. Loss of lipocalin 10 exacerbates diabetes-induced cardiomyopathy *via* disruption of Nr4a1-mediated anti-inflammatory response in macrophages. *Front Immunol* 2022;**13**:930397.
32. Guardado S, Ojeda-Juárez D, Kaul M, Nordgren TM. Comprehensive review of lipocalin 2-mediated effects in lung inflammation. *Am J Physiol Lung Cell Mol Physiol* 2021;**321**:L726–L733.
33. Jaberi SA, Cohen A, D'Souza C, Abdulrazzaq YM, Ojha S, Bastaki S, Adeghate EA. Lipocalin-2: structure, function, distribution and role in metabolic disorders. *Biomed Pharmacother* 2021;**142**:112002.
34. Wang P, Mu X, Zhao H, Li Y, Wang L, Wolfe V, Cui SN, Wang X, Peng T, Zingarelli B, Wang C, Fan GC. Administration of GDF3 into septic mice improves survival *via* enhancing LXRα-mediated macrophage phagocytosis. *Front Immunol.* 2021;**12**:647070.
35. Wang J, Niu N, Xu S, Jin ZG. A simple protocol for isolating mouse lung endothelial cells. *Sci Rep* 2019;**9**:1458.
36. Gardner GT, Travers JG, Qian J, Liu GS, Haghighi K, Robbins N, Jiang M, Li Y, Fan GC, Rubinstein J, Blaxall BC, Kranias EG. Phosphorylation of Hsp20 promotes fibrotic remodeling and heart failure. *JACC Basic Transl Sci* 2019;**4**:188–199.
37. Mu X, Wang X, Huang W, Wang RT, Essandoh K, Li Y, Pugh AM, Peng J, Deng S, Wang Y, Caldwell CC, Peng T, Yu KJ, Fan GC. Circulating exosomes isolated from septic mice induce cardiovascular hyperpermeability through promoting podosome cluster formation. *Shock* 2018;**49**:429–441.
38. Wang L, Mehta S, Ahmed Y, Wallace S, Pape MC, Gill SE. Differential mechanisms of septic human pulmonary microvascular endothelial cell barrier dysfunction depending on the presence of neutrophils. *Front Immunol* 2018;**9**:1743.
39. Wang L, Li Y, Wang X, Wang P, Essandoh K, Cui S, Huang W, Mu X, Liu Z, Wang Y, Peng T, Fan GC. GDF3 protects mice against sepsis-induced cardiac dysfunction and mortality by suppression of macrophage pro-inflammatory phenotype. *Cells* 2020;**9**:120.

40. Zhang X, Wang X, Zhu H, Kranias EG, Tang Y, Peng T, Chang J, Fan GC. Hsp20 functions as a novel cardiokine in promoting angiogenesis via activation of VEGFR2. *PLoS One* 2012;**7**: e32765.
41. Suzuki K, Lareyre JJ, Sánchez D, Gutierrez G, Araki Y, Matusik RJ, Orgebin-Crist MC. Molecular evolution of epididymal lipocalin genes localized on mouse chromosome 2. *Gene* 2004;**339**:49–59.
42. Wolfien M, Galow AM, Müller P, Bartsch M, Brunner RM, Goldammer T, Wolkenhauer O, Hoeflich A, David R. Single-nucleus sequencing of an entire mammalian heart: cell type composition and velocity. *Cells* 2020;**9**:318.
43. Hariri G, Joffre J, Leblanc G, Bonsey M, Lavillegrand JR, Urbina T, Guidet B, Maury E, Bakker J, Ait-Oufella H. Narrative review: clinical assessment of peripheral tissue perfusion in septic shock. *Ann Intensive Care* 2019;**9**:37.
44. Tang N, Tian W, Ma GY, Xiao X, Zhou L, Li ZZ, Liu XX, Li CY, Wu KH, Liu W, Wang XY, Gao YY, Yang X, Qi J, Li D, Liu Y, Chen WS, Gao J, Li XQ, Cao W. TRPC channels blockade abolishes endotoxemic cardiac dysfunction by hampering intracellular inflammation and Ca^{2+} leakage. *Nat Commun* 2022;**13**:7455.
45. Redl B, Habeler M. The diversity of lipocalin receptors. *Biochimie* 2022;**192**: 22–29.
46. Mineo C. Lipoprotein receptor signaling in atherosclerosis. *Cardiovasc Res* 2020;**116**: 1254–1274.
47. Wittchen ES. Endothelial signaling in paracellular and transcellular leukocyte transmigration. *Front Biosci* 2009;**14**:2522–2545.
48. Ghim M, Alpresa P, Yang SW, Braakman ST, Gray SG, Sherwin SJ, van Reeuwijk M, Weinberg PD. Visualization of three pathways for macromolecule transport across cultured endothelium and their modification by flow. *Am J Physiol Heart Circ Physiol* 2017; **313**:H959–H973.
49. Hartsock A, Nelson WJ. Adherens and tight junctions: structure, function and connections to the actin cytoskeleton. *Biochim Biophys Acta* 2008;**1778**:660–669.
50. Woo JA, Boggess T, Uhlar C, Wang X, Khan H, Cappos G, Joly-Amado A, De Narvaez E, Majid S, Minamide LS, Bamburg JR, Morgan D, Weeber E, Kang DE. RanBP9 at the intersection between cofilin and aβ pathologies: rescue of neurodegenerative changes by RanBP9 reduction. *Cell Death Dis* 2015;**6**:e1676.

Translational perspective

Many human disease conditions (i.e. virus infection, bacterial sepsis, and metabolic disorders) can trigger systemic inflammation, which usually causes vascular hyper-permeability and thereby, organ oedema/failure and patient mortality. This study, using both loss-of- and gain-of-function approaches, elucidates Lcn10 as a potent and novel regulator of vascular permeability and a new protector against inflammation-induced cardiovascular dysfunction. Mechanistically, we define that Lcn10 interacts with LDL receptor-related protein 2 (LRP2), leading to the activation of its downstream Ssh1-Cofilin signalling in endothelial cells and consequently, protects endothelial integrity. Our findings may provide novel strategies for the treatment of inflammation-related diseases.